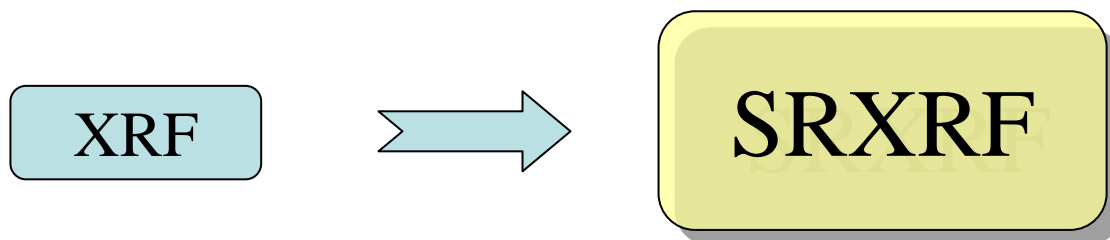




# *SR excited X-ray Fluorescence Analysis (SRXRF)*



17 Sept., 2007  
Cheiron School

Atsuo IIDA  
Photon Factory

- *Principles of SRXRF*
- *Micro-beam Analysis*
- *Applications of SRXRF*



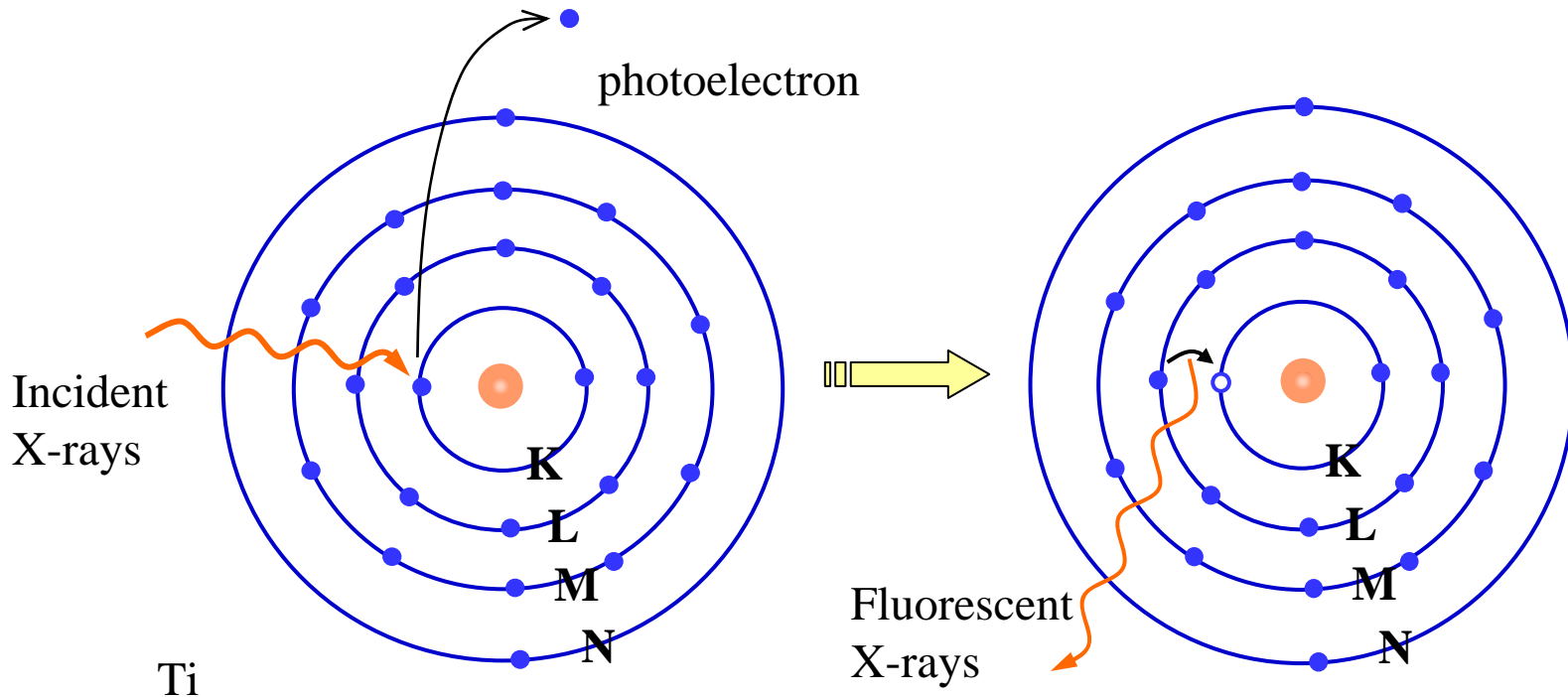
# **XRF Primer**

Cheiron School 2007 by AOFSRR

A.Iida (PF)



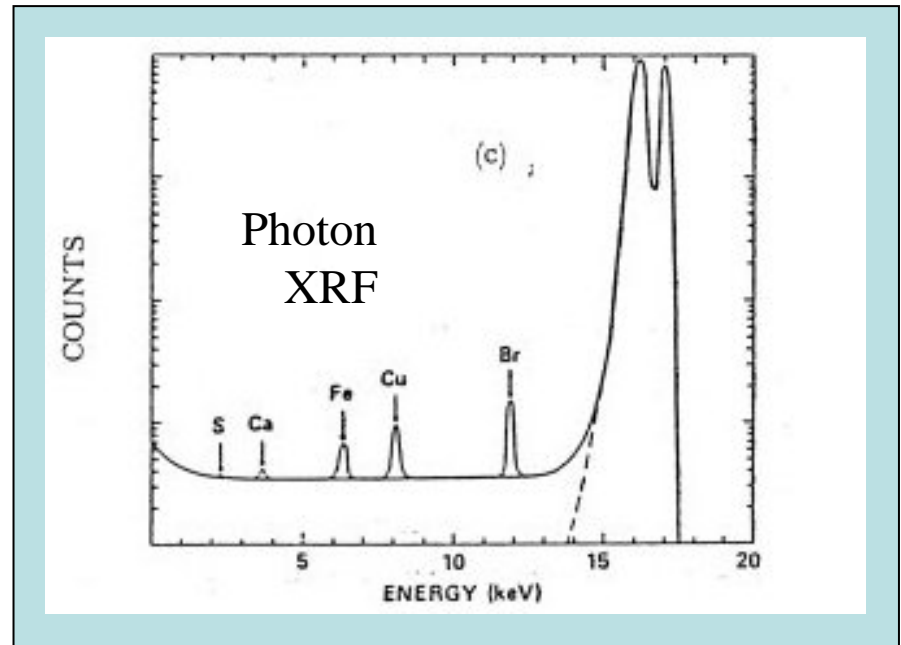
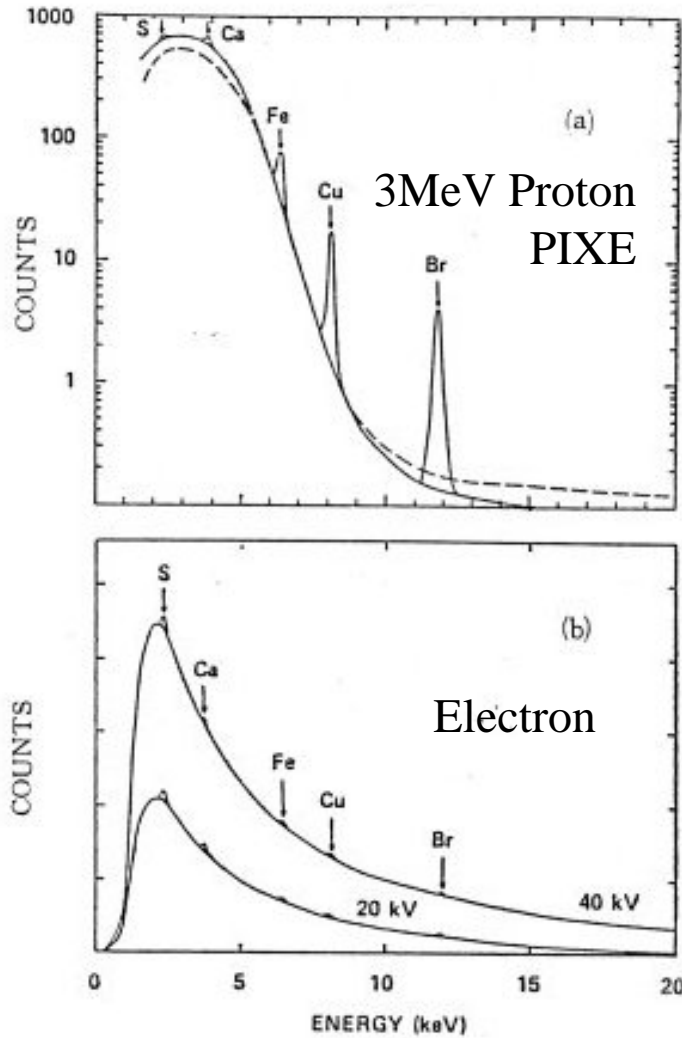
# X-ray Fluorescence Analysis



Excitation sources	Analytical techniques
X-rays	XRF (X-ray fluorescence analysis)
Electron	EPMA (Electron probe micro analyzer)
Charged particle	PIXE (Particle/Proton Induced X-ray emission)



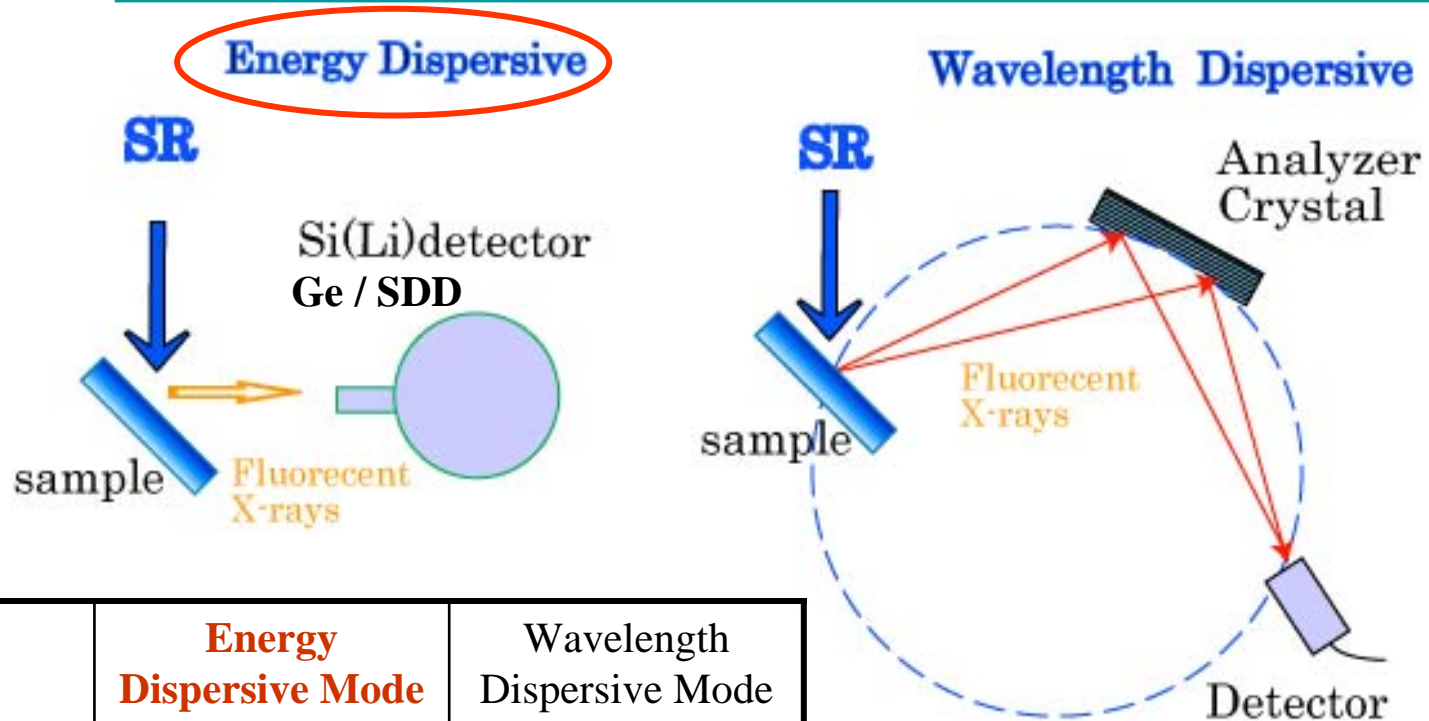
# *X-ray Emission by Proton, Electron and Photon Excitation*



after C.J.Spaks, Jr  
In "Synchrotron Radiation Research" (1980)



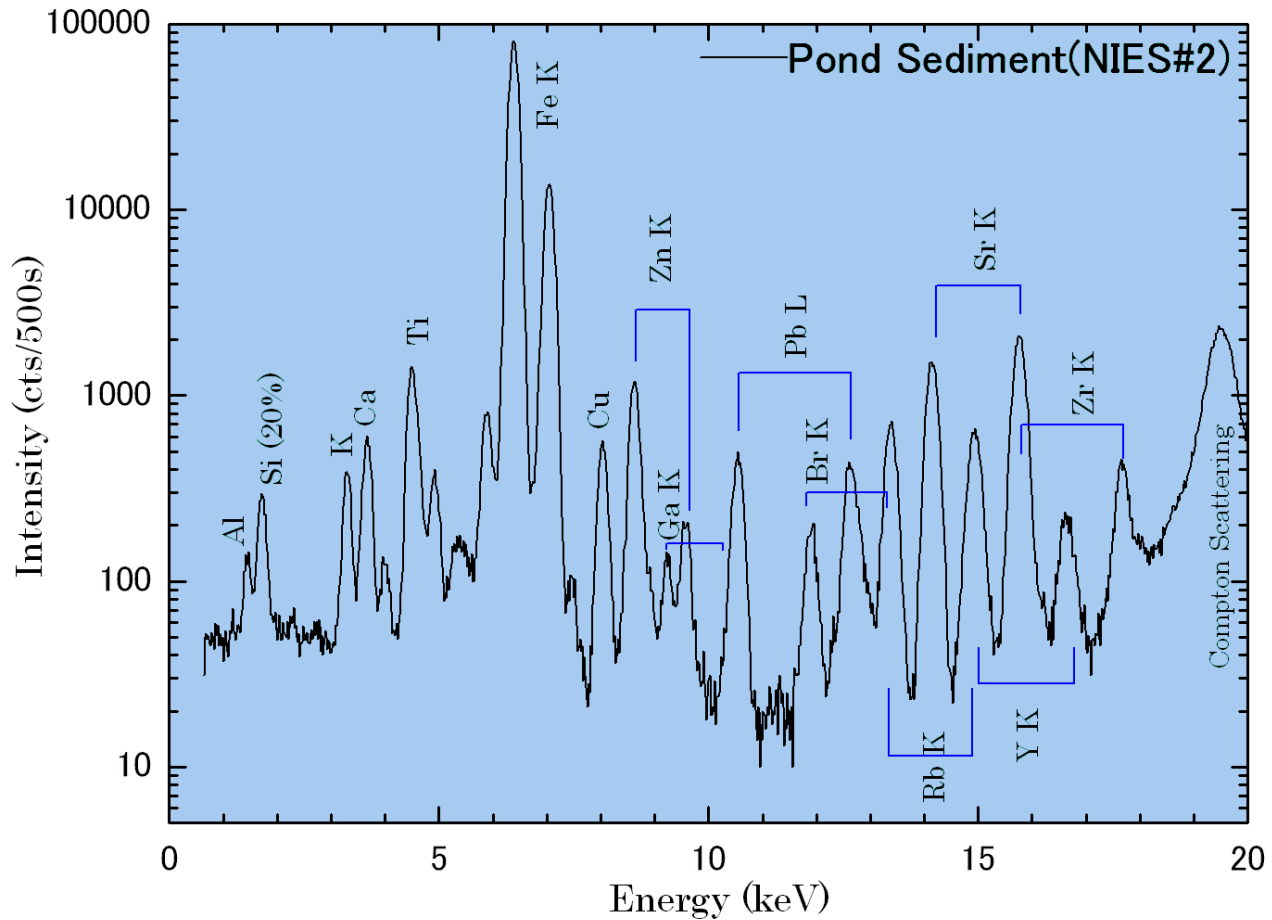
# Energy Dispersive Mode vs. Wavelength Dispersive Mode



	<b>Energy Dispersive Mode</b>	Wavelength Dispersive Mode
Advantage	<ul style="list-style-type: none"> <li>• <u>High Efficiency</u></li> <li>• Multi-elemental detection</li> </ul>	<ul style="list-style-type: none"> <li>• High resolution</li> <li>• High S/B</li> </ul>
Disadvantage	<ul style="list-style-type: none"> <li>• <u>Low resolution</u></li> <li>• Scattering background</li> </ul>	<ul style="list-style-type: none"> <li>• Low efficiency</li> </ul>



# SRXRF Pond Sediment (池底質)



**Energy**  
**Dispersive Mode**

Fe 6%, Br 17ppm, Zn 343 ppm



# X-ray fluorescence intensity II

Total integrated fluorescence intensity by monochromatic excitation

$$P_i(\lambda) = q \cdot E_i \cdot C_i \cdot \{1 - \exp(-\rho \cdot h \cdot A)\} \frac{\mu_{i\lambda} \cdot I_\lambda \cdot d\lambda}{A \cdot \sin \alpha}$$

$$E_i = \frac{\gamma_K - 1}{\gamma_K} \cdot \omega_K \cdot g_{K\alpha}$$

$$A = \frac{\mu_{s,\lambda}}{\sin \alpha} + \frac{\mu_{s,\lambda i}}{\sin \beta}$$

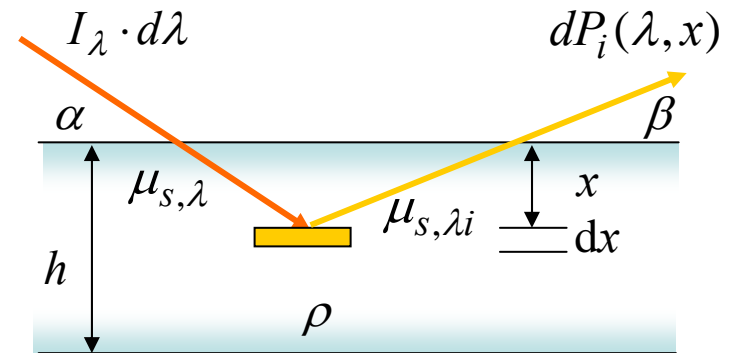
Thick Specimen ( $h \Rightarrow \infty$ )

$$I_{i,s}(\lambda) = q \cdot E_i \cdot C_i \cdot \frac{\mu_{i\lambda} \cdot U_\lambda}{A \cdot \sin \alpha}$$

Thin Specimen ( $h \Rightarrow 0$ )

$$I_{i,s}(\lambda) = q \cdot E_i \cdot C_i \cdot \rho \cdot h \cdot \frac{\mu_{i\lambda} \cdot U_\lambda}{\sin \alpha}$$

$C_i$  : Concentration     $h$  : Thickness



$\mu_{i\lambda}$  : mass absorption coefficient of element  $i$  for incident X-ray energy of  $\lambda$



# Sensitivity & Detection Limit (IUPAC)

## Analytical calibration curve

- The relation of the measured values ( $x$ ) to the concentration ( $c$ ) (or any quantity( $q$ )) of the material.
- $x=g(c)$  or  $x=g(q)$

## • Sensitivity $S$

- the increment of the measured value  $\Delta x$  for the unit change of the concentration  $\Delta c$ .

$$S = \frac{dx}{dc}$$

## • Limit of detection / minimum detection limit

$$c_L (q_L)$$

- the minimum concentration of the analyte element or minimum quantity which can be measured

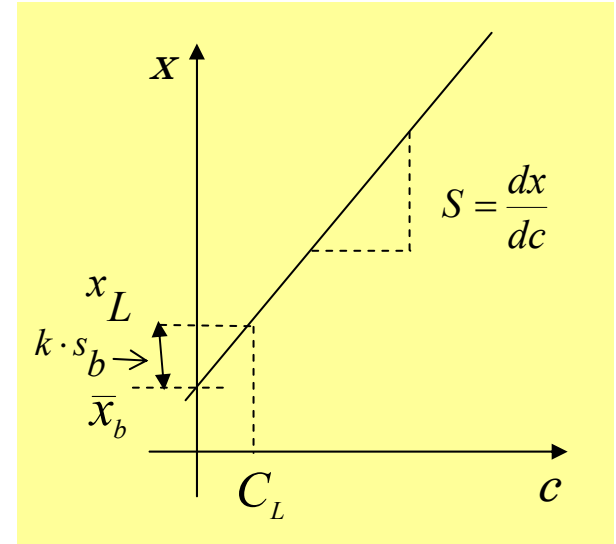
$$x_L = \bar{x}_b + k \cdot s_b$$

$\bar{x}_b$  Average value for the blank

$s_b$  Standard deviation for the blank

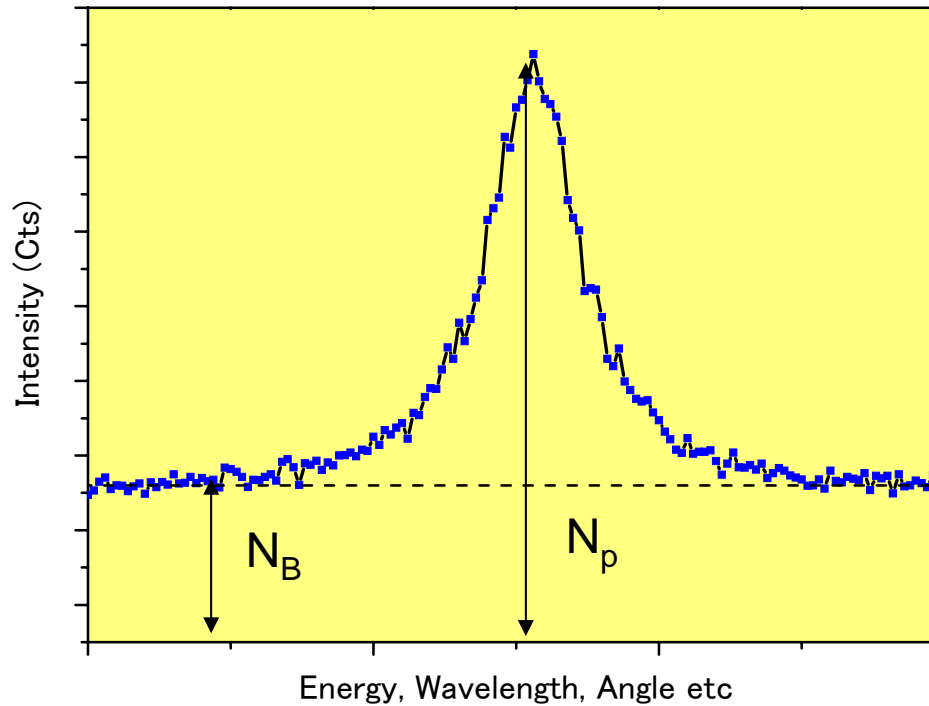
$k$  Empirical value (=3)

$$C_L = \frac{x_L - \bar{x}_b}{S}$$





# MDL (Minimum detection limit)



Minimum detection  
limit (MDL)

$$k = \frac{3C\sqrt{N_B}}{N_p - N_B}$$

Minimum quantification  
limit (MQL)  $(2k \sim 3.3k)$



# SR XRF

Cheiron School 2007 by AOFSRR

A.Iida (PF)



# *Synchrotron radiation excited XRF* *-SRXRF-*

## Advantages of conventional XRF

- Nondestructive
- Wide dynamic range  
major ~ trace
- User-friendly instruments
- Multi-elemental analysis
- High accuracy
- Easy to analyze



## Advantages of SRXRF

- **High sensitivity**  
ng=>fg, ppm=>ppb
- **Micro-beam analysis**  
mm =>  $\mu\text{m}$
- **Chemical state analysis**
- **Total reflection analysis**  
 $10^{15}\text{atoms/cm}^2$   
=>  $10^8\text{atoms/cm}^2$



# SR Properties and SRXRF

## 1) High Brilliance Source

(small size and high collimation X-ray source)

strong intensity (high density)

=>signal enhancement

high collimation

=>micro beam analysis (focusing optics)

=>total reflection XRF

## 2) Linear polarization

(p polarization + 90° arrangement) => background reduction

## 3) White (bending magnet), quasi-monochromatic (Undulator) X-rays

monochromatic X-rays

=> background reduction

(monochromator)

=> selective excitation

(S/B optimization / Resolving overlapping peak)

continuous energy scanning

=>XAFS

(Chemical state analysis)

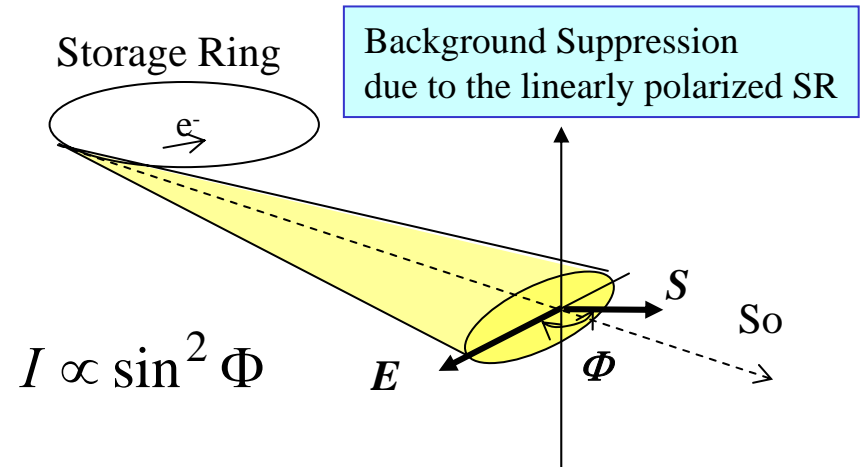
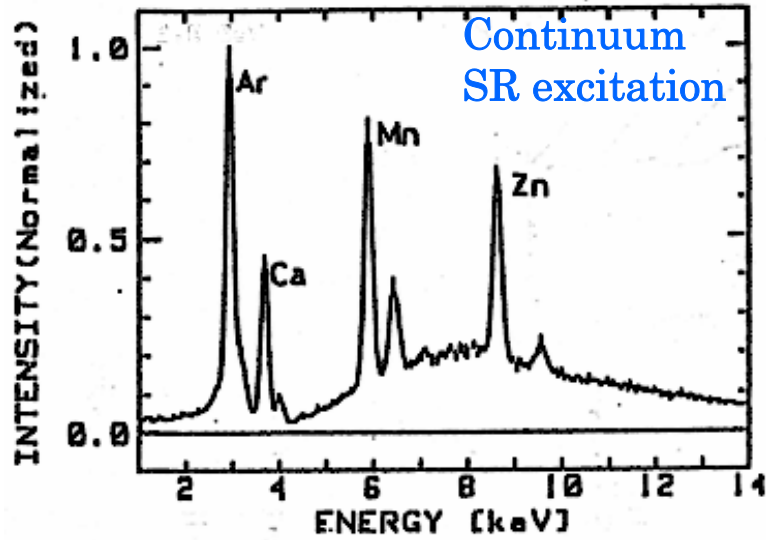
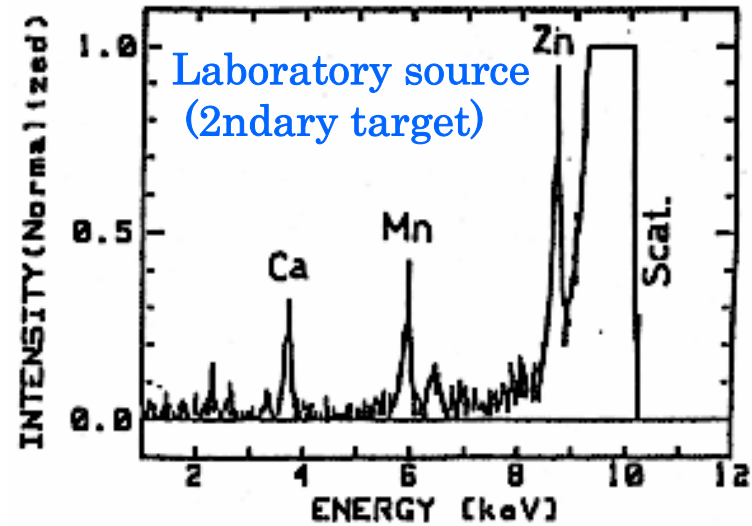
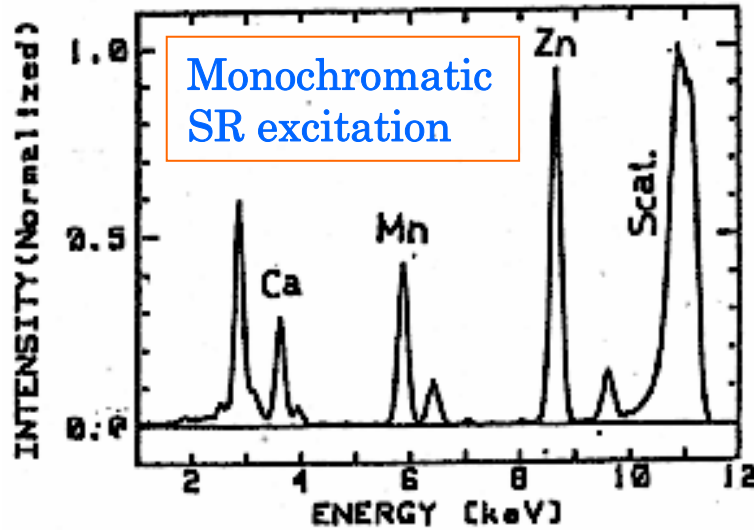
## 4) High and low energy X-ray excitation

=>heavy & light trace elements analysis



# Monochromatic SR Excitation advantages: High Signal / Background ratio

(Sample: Chelete resin beads)

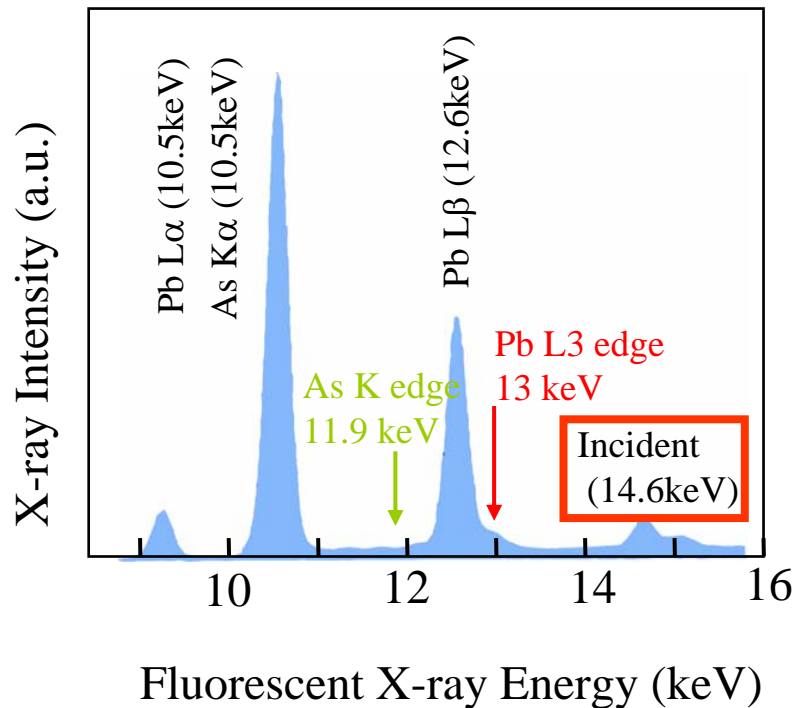




# Selective Excitation :

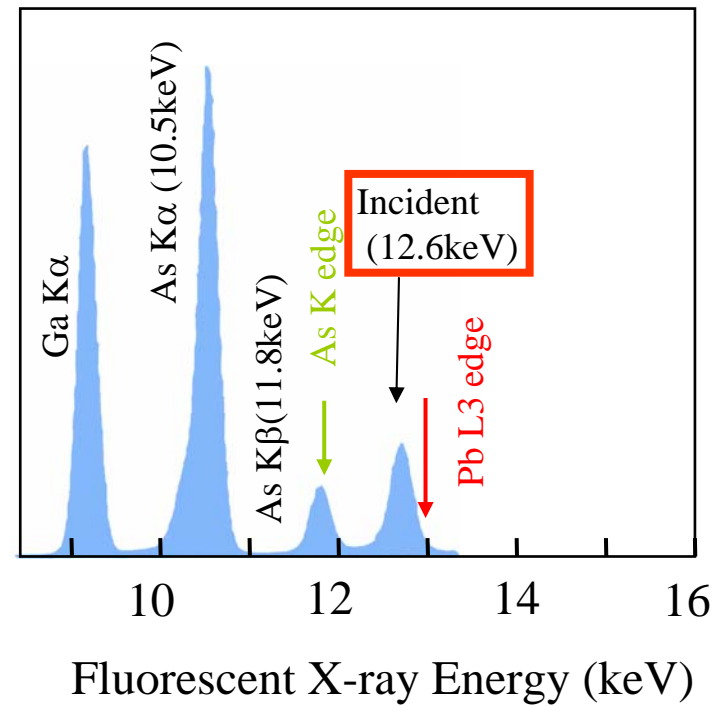
## Resolving overlapping peaks: PbL $\alpha$ vs. As K $\alpha$ Case

As Kedge < PbL3 edge < E<sub>0</sub>



Both As K and Pb L are excited.

As Kedge < E<sub>0</sub> < PbL3 edge



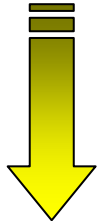
As K series alone is excited.  
=>As quantification becomes possible.



# Hard X-ray Advantage: Heavy elements analysis

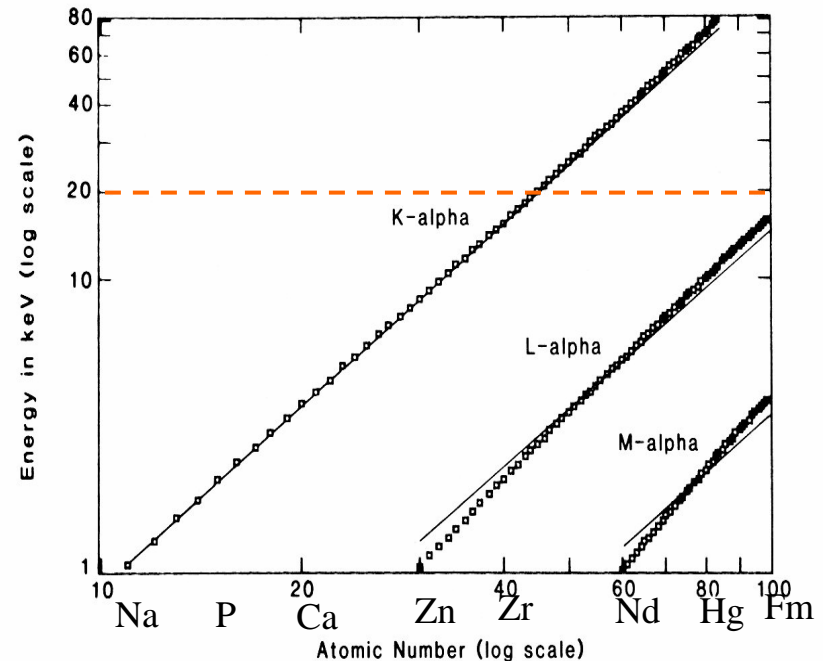
- Disadvantage of L series analysis
  - Complicated lines  $L\alpha, \beta, \gamma, l, s$
  - Peak overlapping between L and K series lines

## High Energy X-ray Excitation



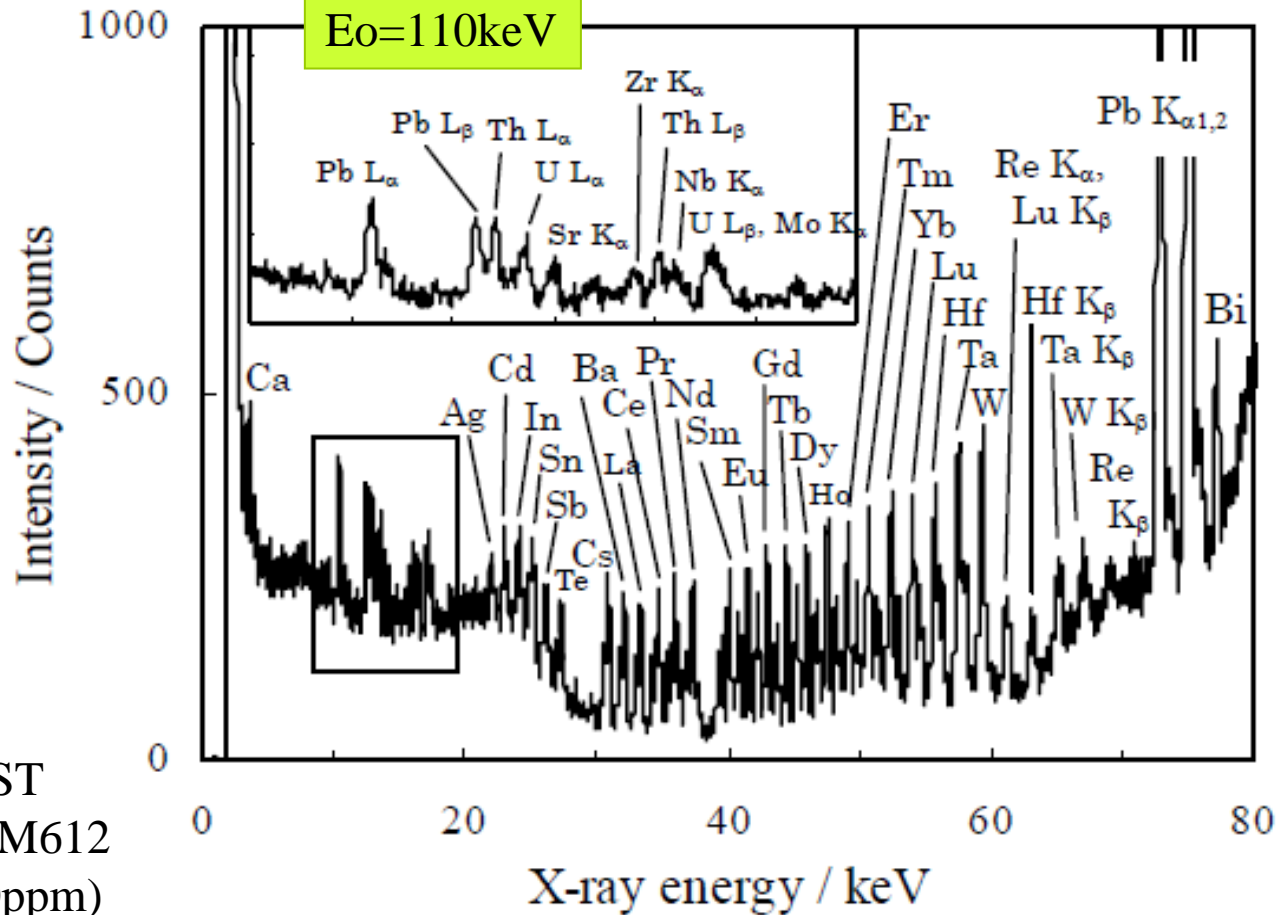
High Energy 3<sup>rd</sup> generation ring  
Wavelength shifter (Wiggler)

- Advantage of K series analysis
  - Simple line Structure  $K\alpha, K\beta$
  - High sensitivity
  - Low absorption (bulk analysis)





# High Energy XRF

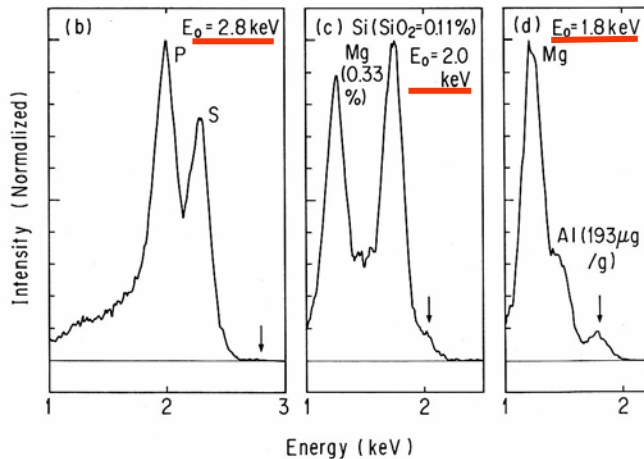
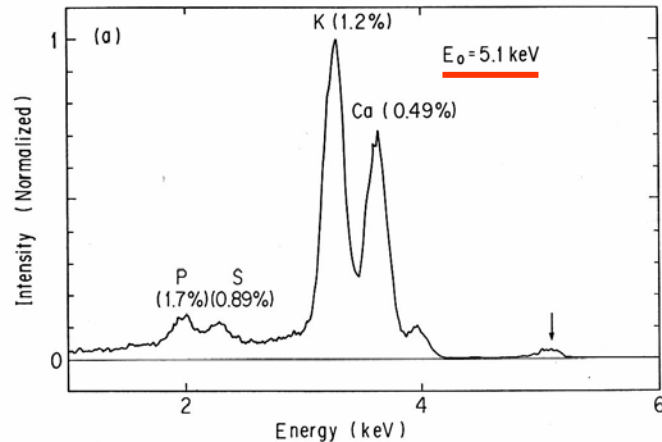


MDL:  
0.1ppm  
10pg

NIST  
SRM612  
(50ppm)



# Light Elements Analysis



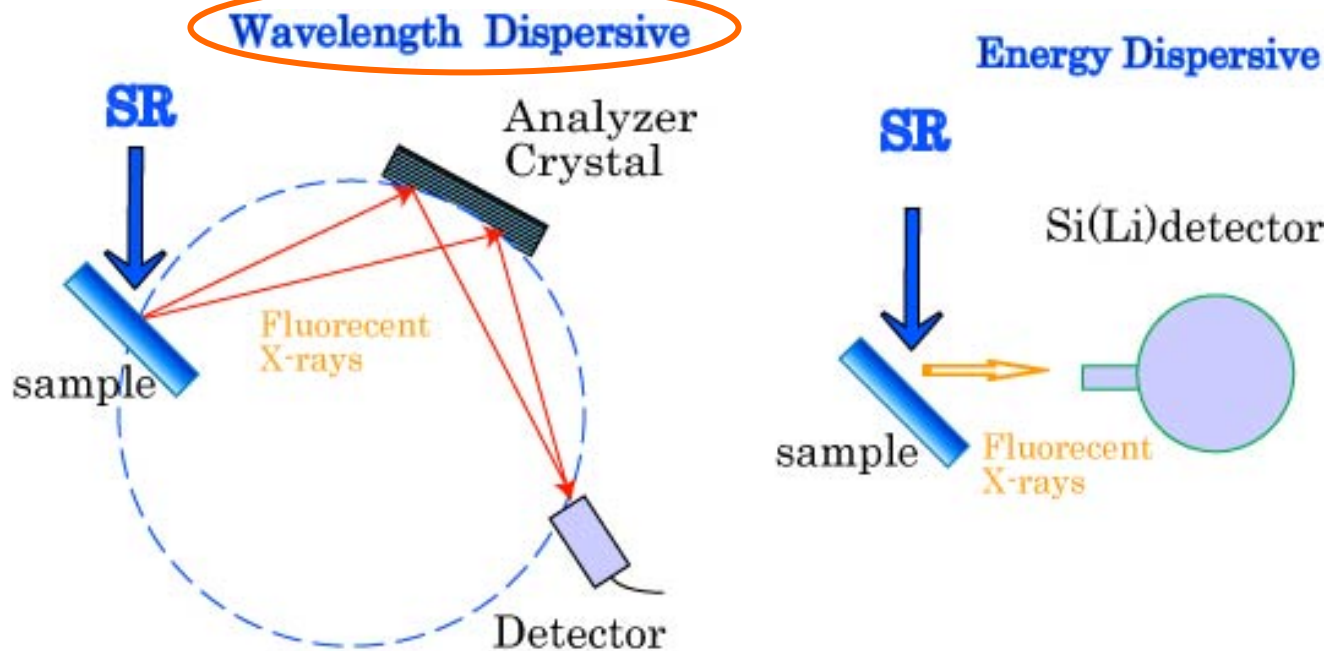
- Light elements (C, N, O, Na~Ca)
  - biological system
  - / material science
- low fluorescence yield
- strong absorption

Soft X-ray Excitation  
from Undulator radiation

Excitation Efficiency is greatly enhanced.



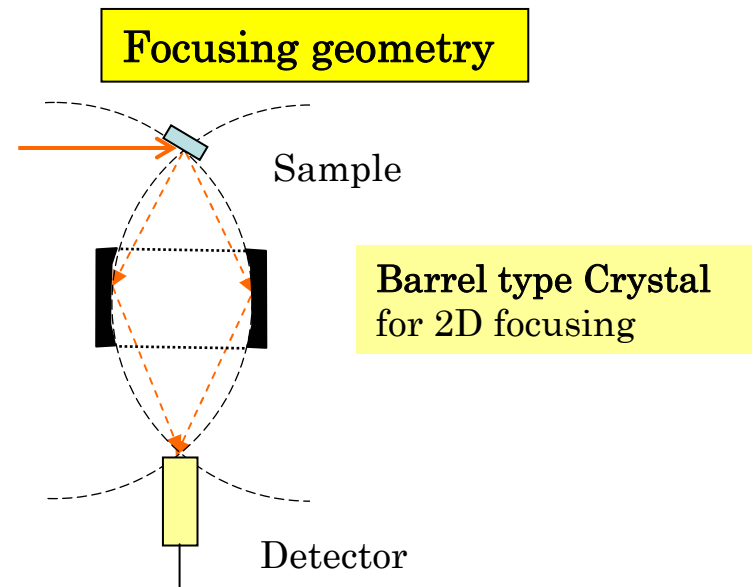
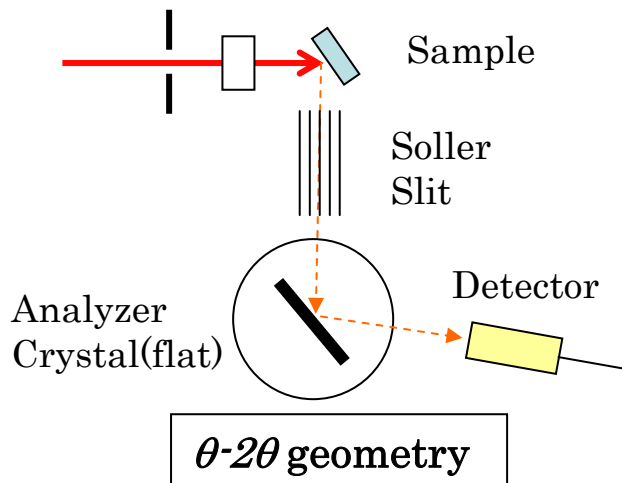
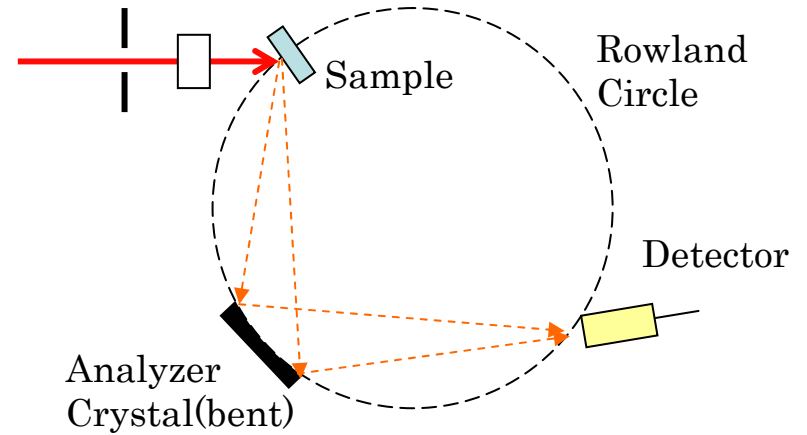
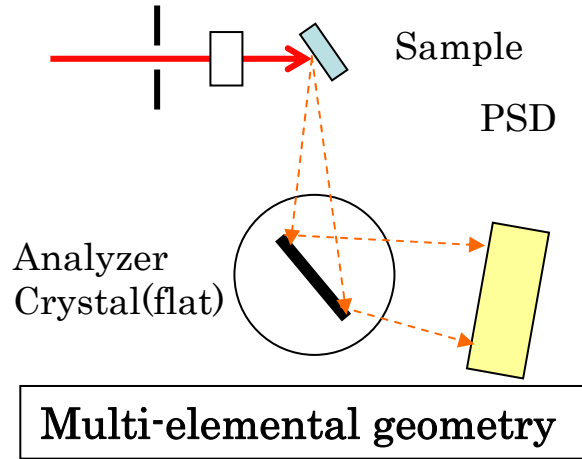
# Wavelength Dispersive XRF



	Wavelength Dispersive	Energy Dispersive
Advantage	<ul style="list-style-type: none"><li>• High resolution (ca. 5 eV~ 50eV eV)</li><li>• High S/B</li></ul>	<ul style="list-style-type: none"><li>• High Efficiency</li><li>• Multi-elemental detection</li></ul>
Disadvantage	<ul style="list-style-type: none"><li>• Low efficiency</li></ul>	<ul style="list-style-type: none"><li>• Low resolution (130 eV)</li><li>• Scattering background</li></ul>

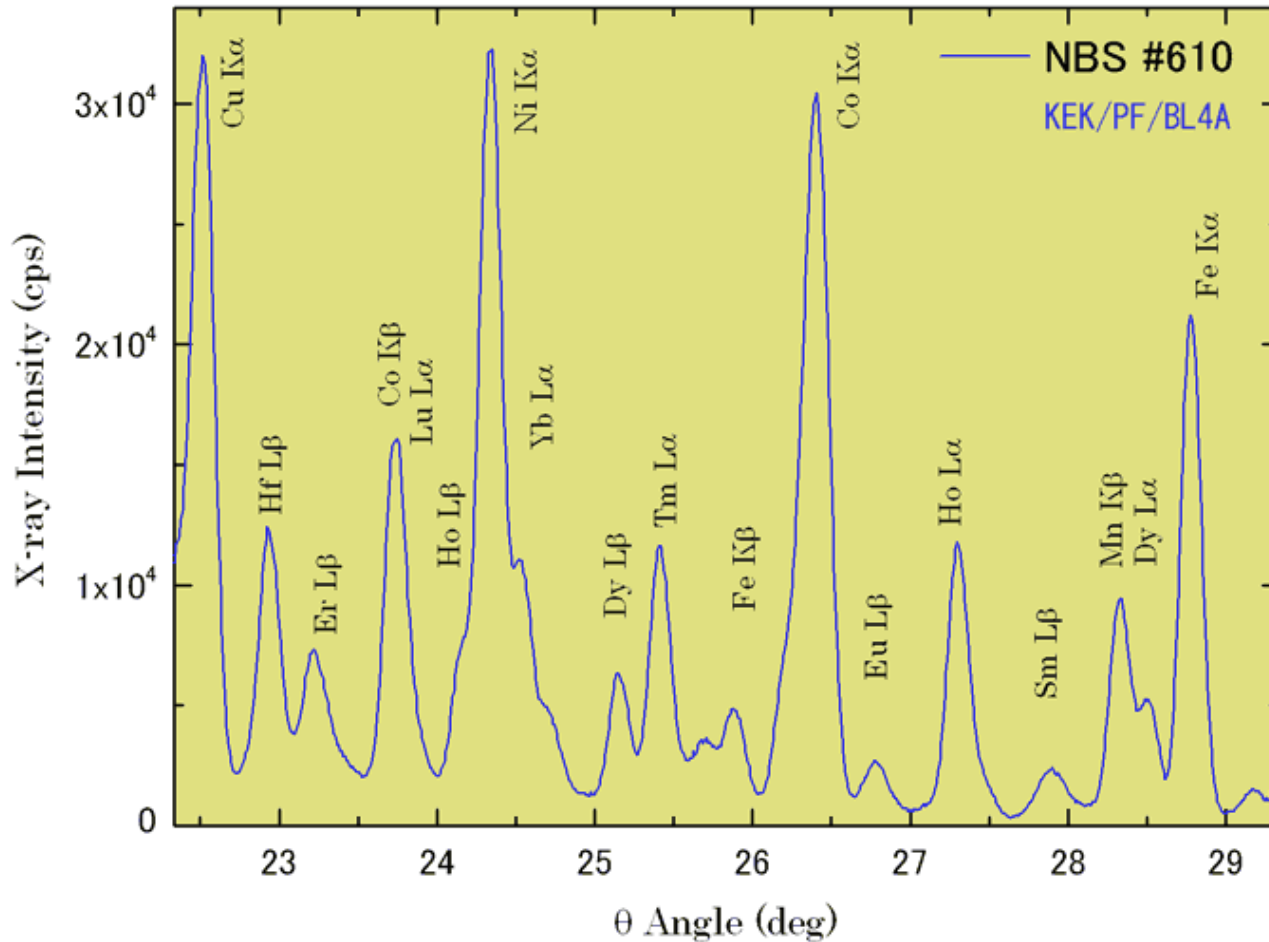


# Wavelength Dispersive Technique





# Wavelength Dispersive XRF Spectrum



Focusing geometry  
Johansson, R=5"  
LiF (200)



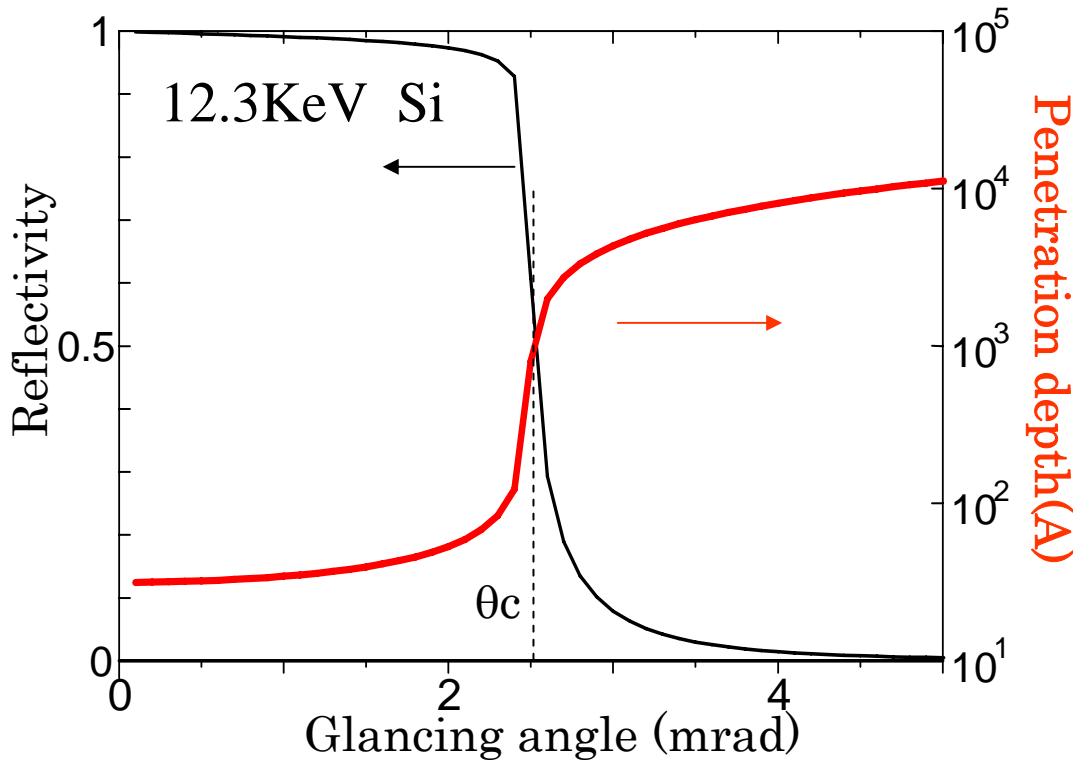
# Grazing Incidence Condition ( High Brilliance Source )

---

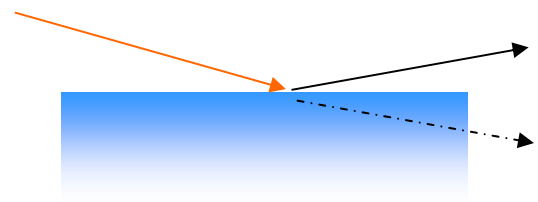
- TXRF total reflection XRF
  - Ultra trace element analysis
- Depth analysis of a single thin layer or a multi-layer
- Reflectometry



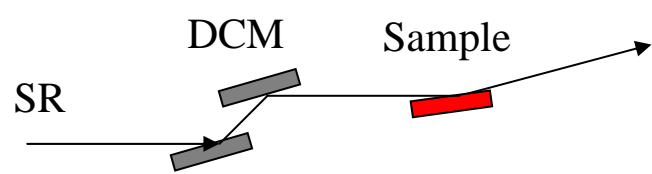
# TXRF for Ultra Trace Element Analysis



Extremely Shallow Penetration Depth



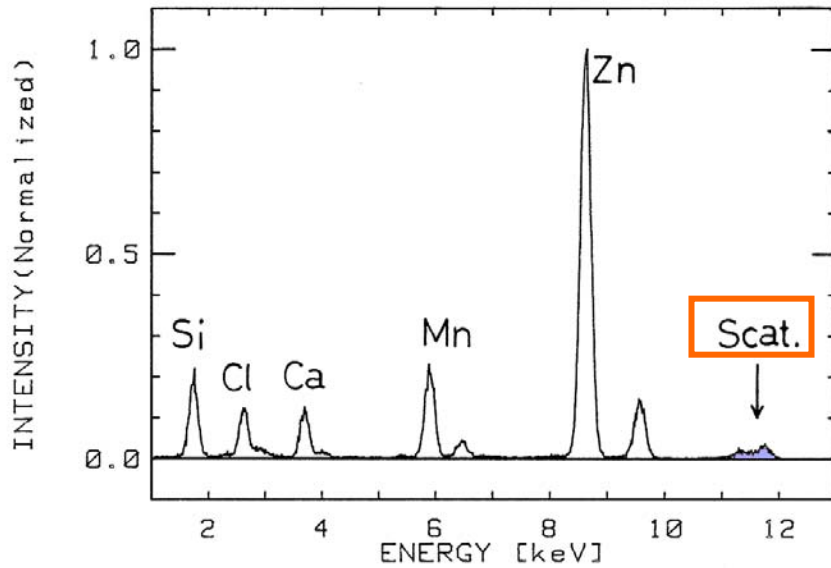
Total Reflection of X-rays at a flat and smooth surface (Si wafer, optical flat .....



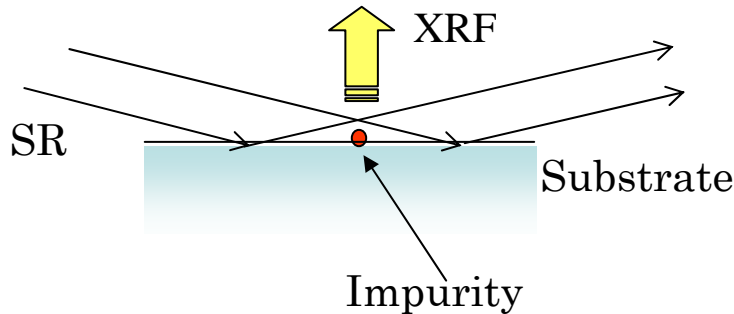
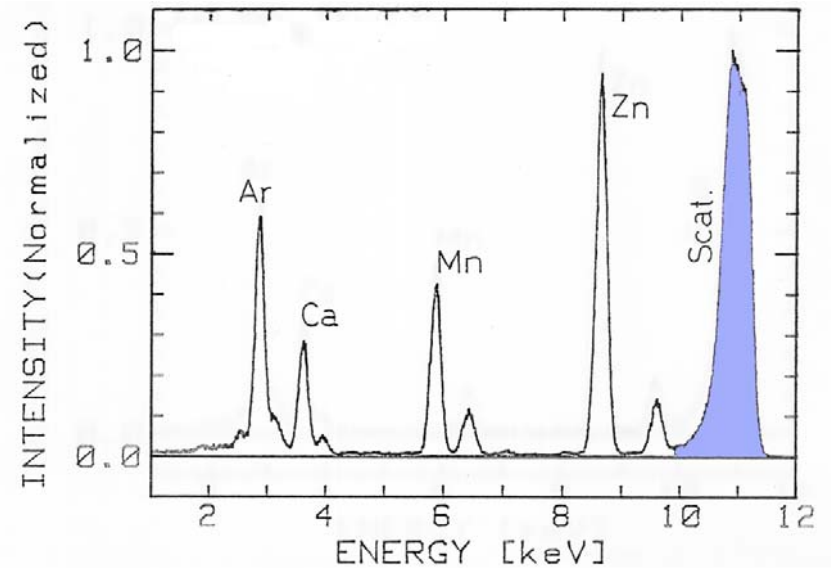


# Total-Reflection X-ray fluorescence analysis Ultra trace element analysis (TXRF)

TXRF



Conventional

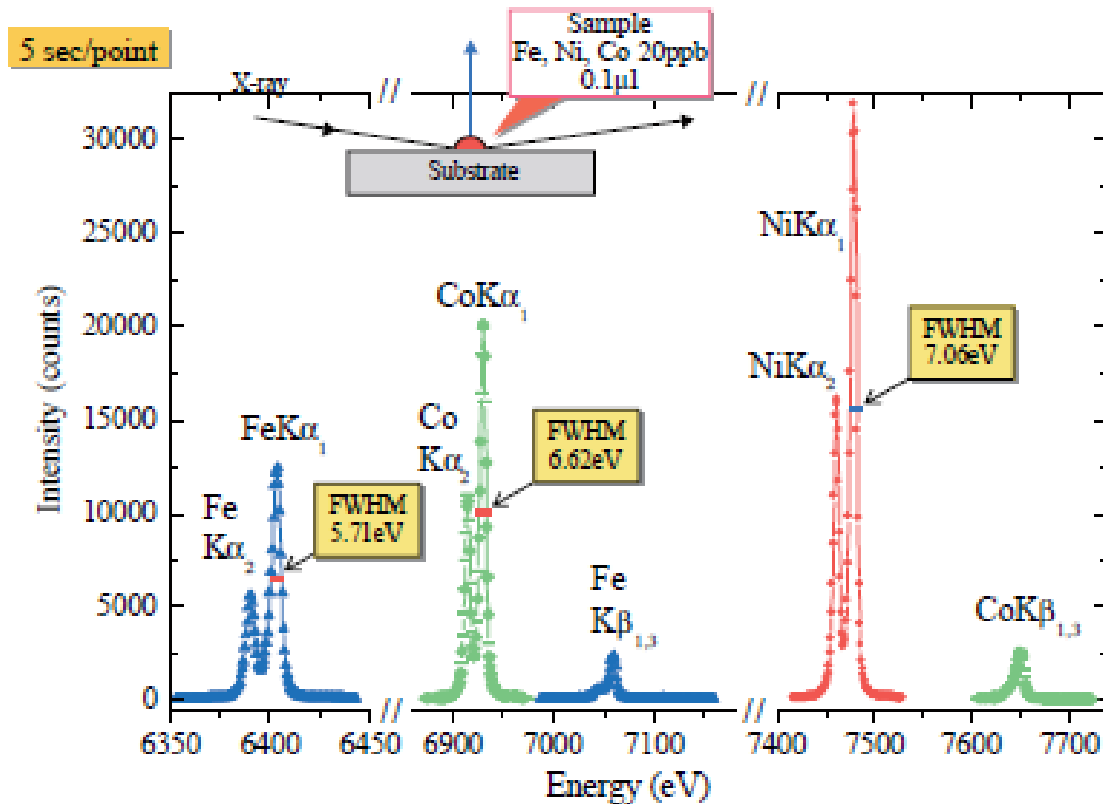


Si wafer

$10^{15}$  atoms/cm<sup>2</sup>  $\Rightarrow$   $10^8$  atoms/cm<sup>2</sup>



# TXRF with Wavelength Dispersive Analyzer



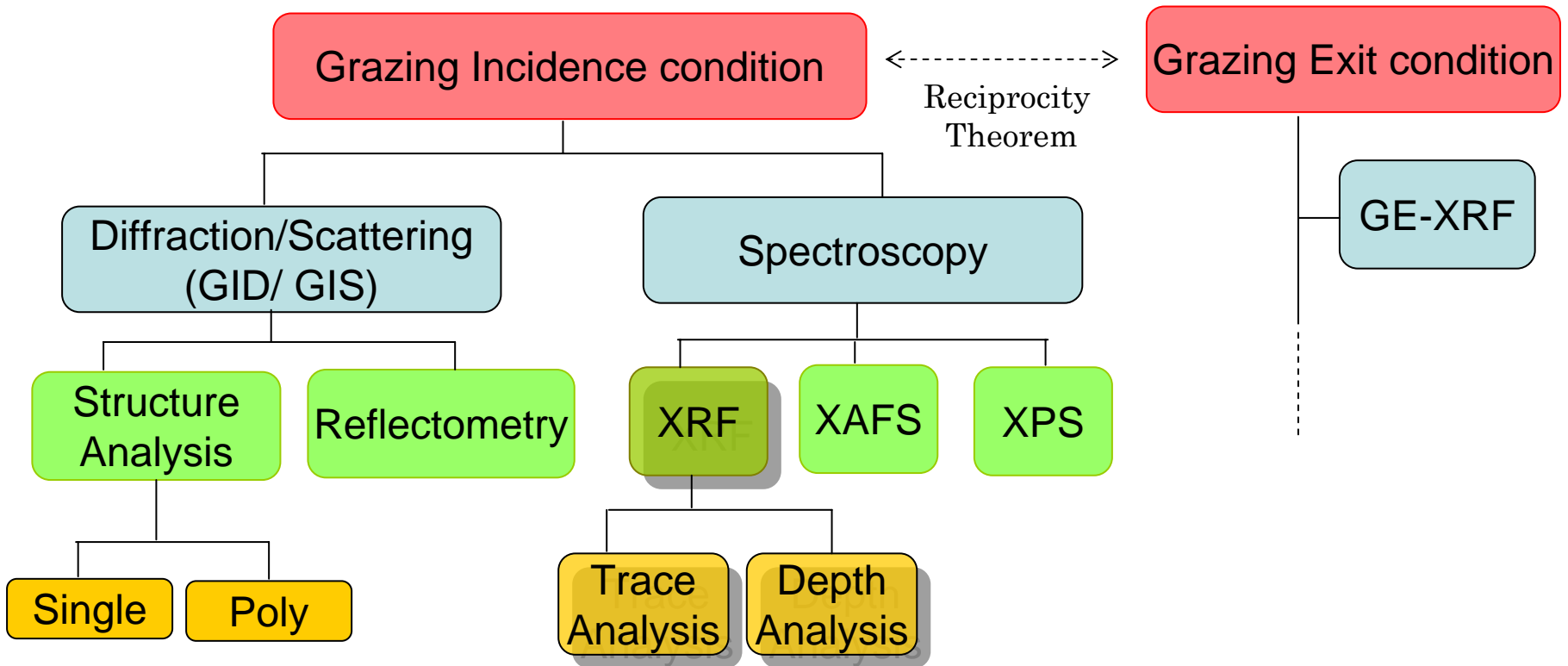
WD-TXRF spectra for trace elements (Ni, Co and Fe, 20 ppb each) in a micro drop (0.1 micro litter).

@ SPring-8 BL40XU  
Ge(220) Johansson  
focusing type WDXRF

K.Sakurai  
SPring-8 Information  
vol.6 No.1(2001)p.35



# X-Ray Surface Analysis using GI Condition



*X-ray Standing Wave*



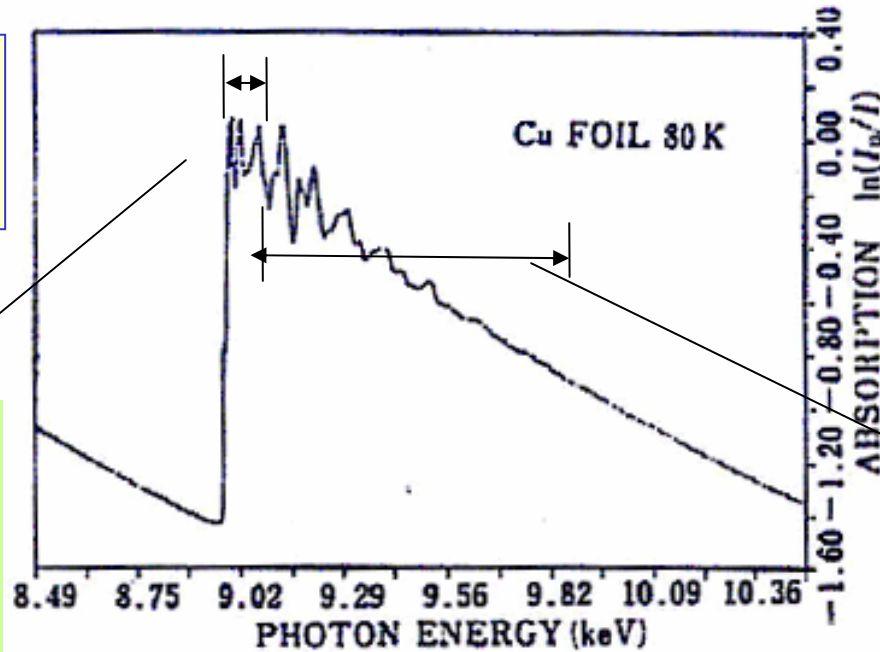
# Chemical State Analysis

- **XAFS (X-ray Absorption Fine Structure)**
  - **XANES**
    - Chemical shift of absorption edge
    - The intensity of the white line
  - EXAFS
    - Local structure
    - Coordination number
- **X-ray Emission**
  - Chemical state analysis
    - Chemical shift of the K or L emission lines
    - Intensity ratio of  $K\alpha$  and  $K\beta$
  - Emission Spectroscopy
    - Resonant inelastic emission spectroscopy
    - .....



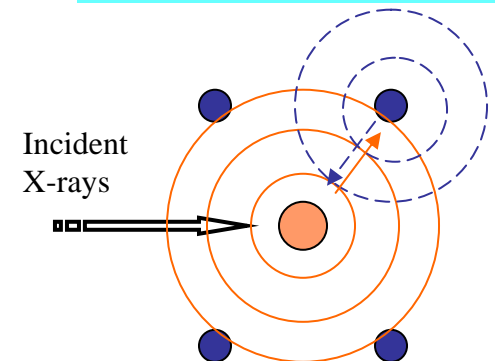
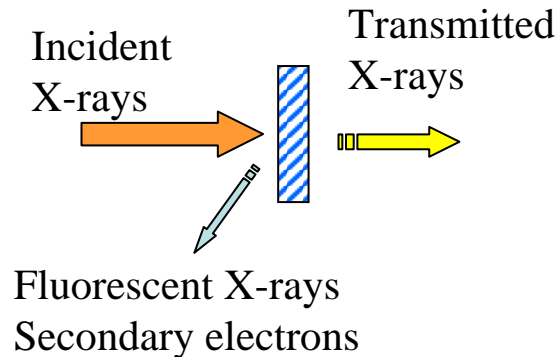
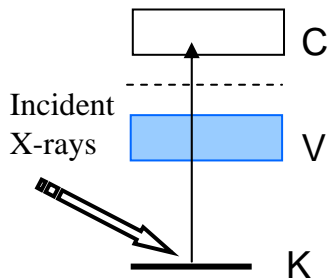
# XAFS (X-ray Absorption Fine Structure)

**Sample:**  
Crystal / amorphous materials



**XANES**  
(X-ray Absorption Near Edge Structure)  
• Electronic state  
• Chemical state

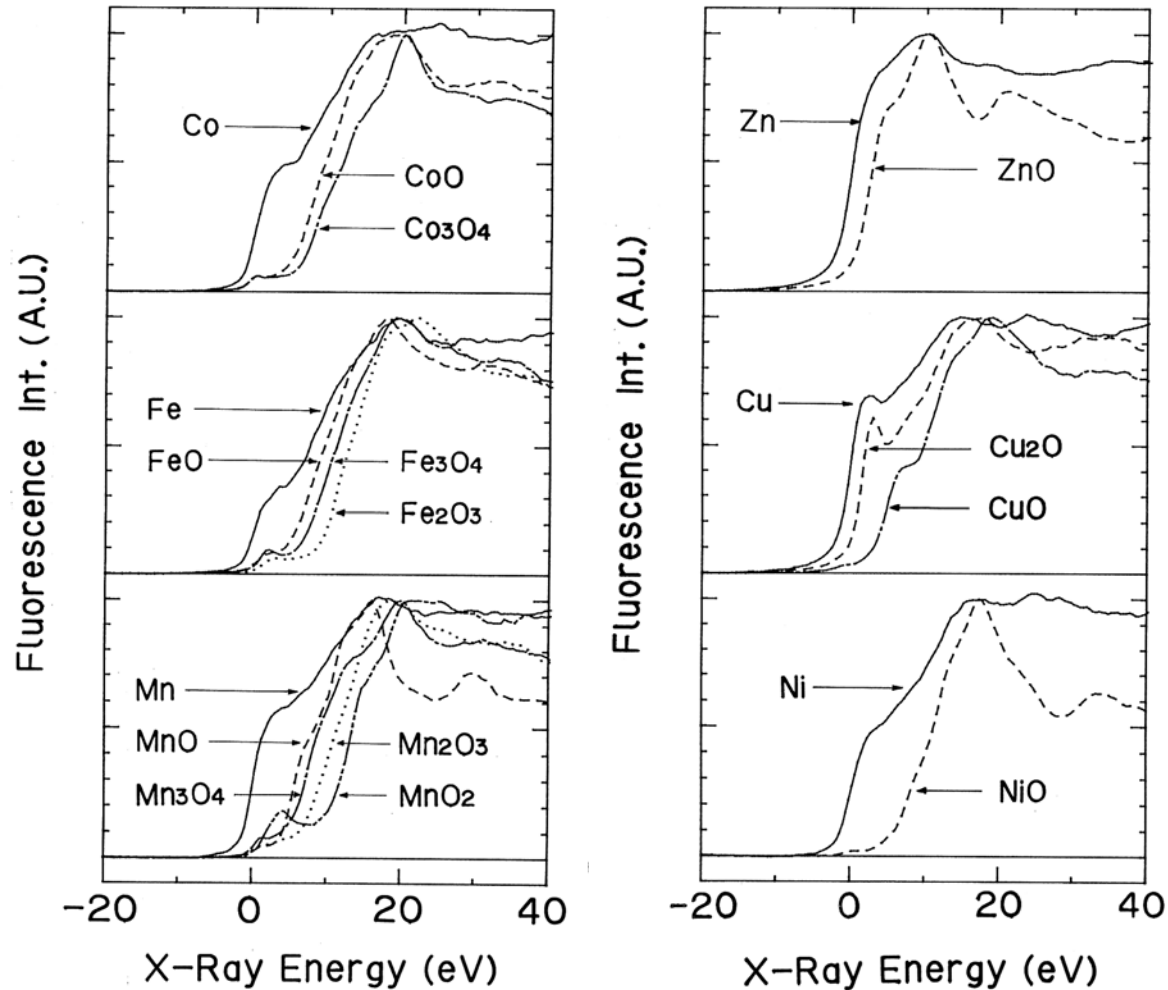
**EXAFS**  
(Extended X-ray Absorption Fine Structure)  
• Local structure  
• Coordination number





# Chemical State analysis by XANES

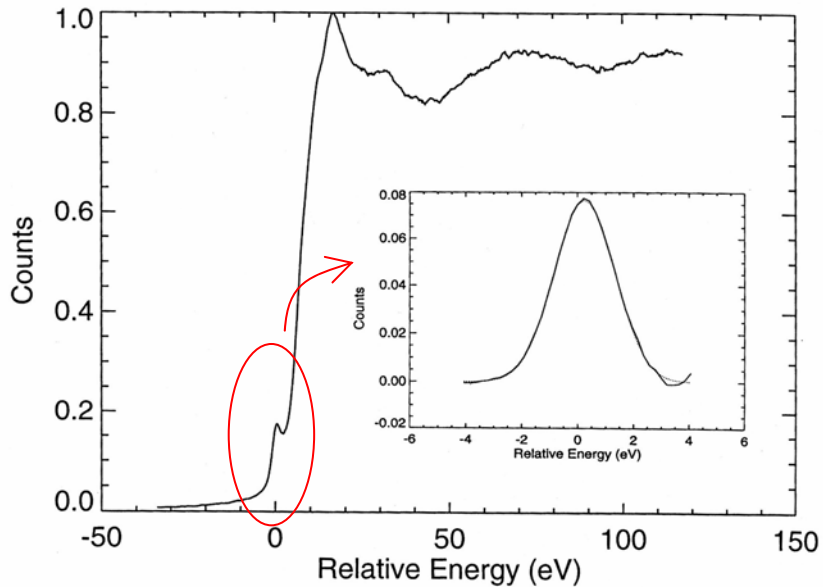
-Chemical Shift of X-ray Absorption edge-



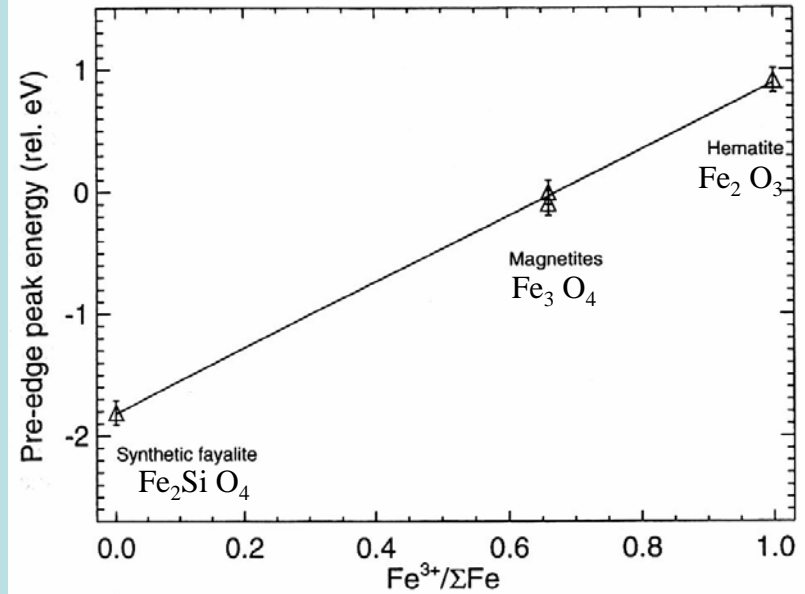
Fingerprint  
Method



# Pre-edge energy analysis: Oxidation state analysis of transition elements



Fe XANES for magnetite



Determination  $Fe^{3+}/\Sigma Fe$  ratio  
by the energy shift of a pre-edge  
in XANES

S. Bajt et al. Geochim. Cosmochim. Acta  
58('94)5209

A linear relationship between pre-edge peak energy and iron oxidation state for oxide and silicate standards.

=> chemical state analysis of transition element in mineral and in the functional materials



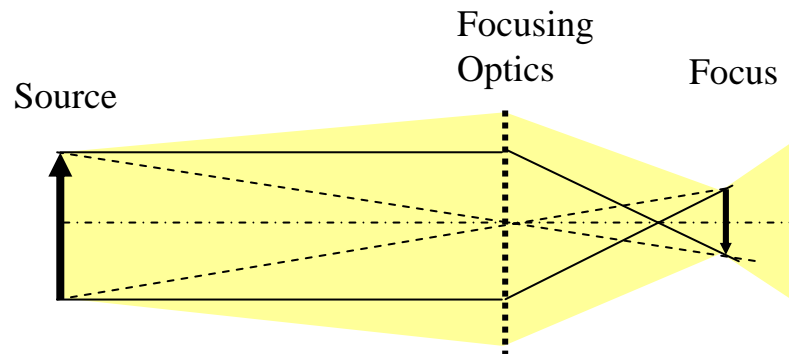
# **Micro-SR XRF**

Cheiron School 2007 by AOFSRR

A.Iida (PF)



# X-ray source and X-ray microbeam



$$1/a + 1/b = 1/f \quad M = b/a$$

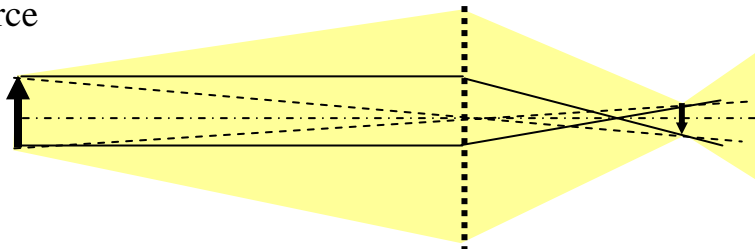
Helmholtz invariant

$$y \times u = y' \times u'$$

$y, y'$  source and focus size

$u, u'$  divergence and convergence angle

Low emittance source



Low emittance source  $\Rightarrow$  small  $y \times u$

Small source size and low divergence

( 3rd generation ring)

$\Rightarrow$  Smaller focus with higher intensity

$\Rightarrow$  micro-beam to nano-beam



# X-ray Focusing Elements

$$n = 1 - \delta - i\beta \quad \delta \sim 10^{-5}$$

X-rays: electromagnetic wave with short wavelength

## Reflection

No chromatic  
aberration

Grazing incidence mirror

spherical / aspherical  
toroidal (bent cylinder)  
elliptical, ellipsoidal  
parabolic, paraboloidal

Capillary (single, poly)

## Diffraction

Energy  
dependence

Fresnel Zone plate

Bragg-Fresnel lens

Crystal (asymmetric reflection / bent crystal)

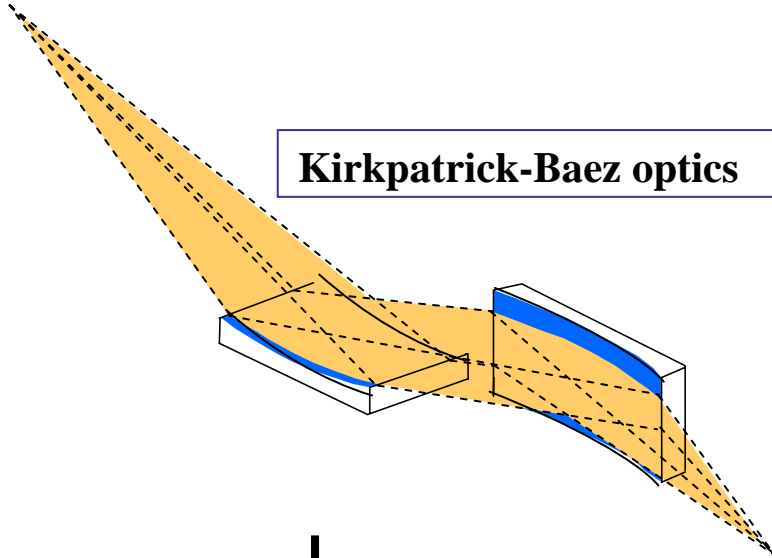
## Refraction

Compound refractive lens

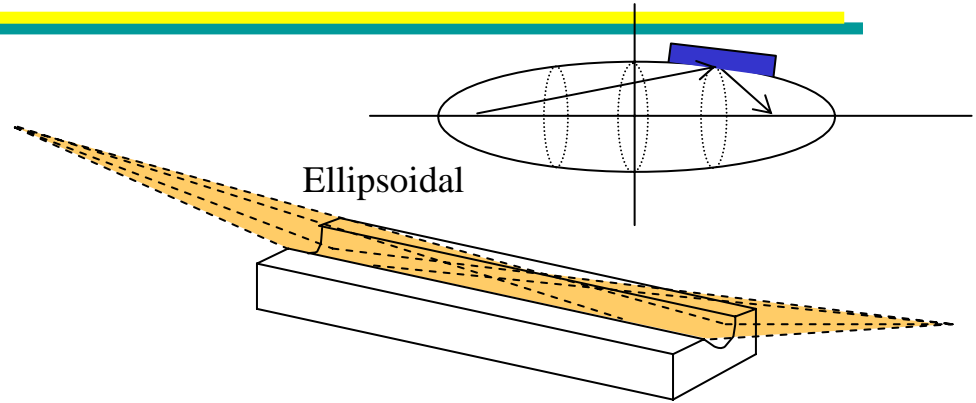


# X-ray microbeam Optics

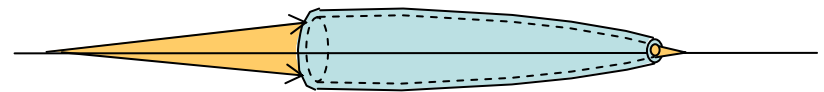
Kirkpatrick-Baez optics



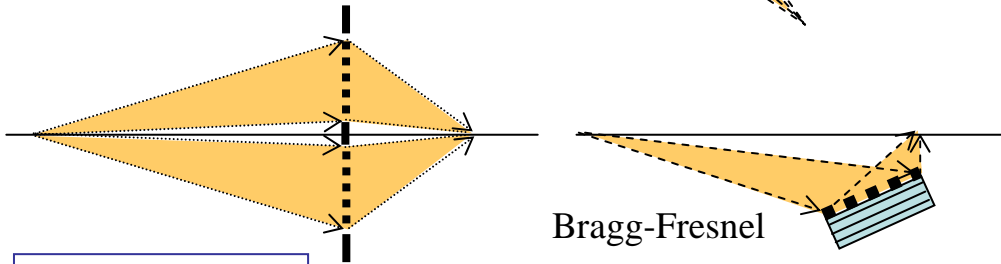
Ellipsoidal



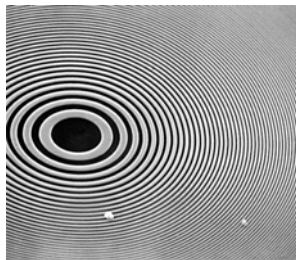
Single tapered capillary



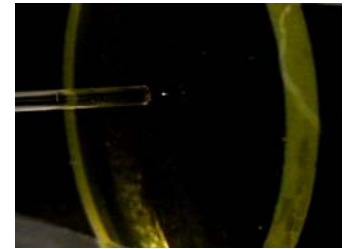
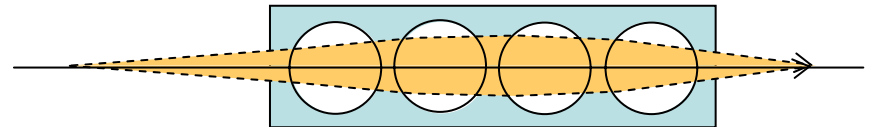
Bragg-Fresnel



Fresnel zone optics



Compound refractive optics





# Fresnel Zone Plate Parameters

## Zone Plate Formulae

$$r_n^2 = n\lambda f + \frac{n^2\lambda^2}{4} \quad (9.9)$$

$$D = 4N\Delta r \quad (9.13)$$

$$f = \frac{4N(\Delta r)^2}{\lambda} \quad (9.14)$$

$$NA = \frac{\lambda}{2\Delta r} \quad (9.15)$$

$$F^\# = \Delta r/\lambda \quad (9.16)$$

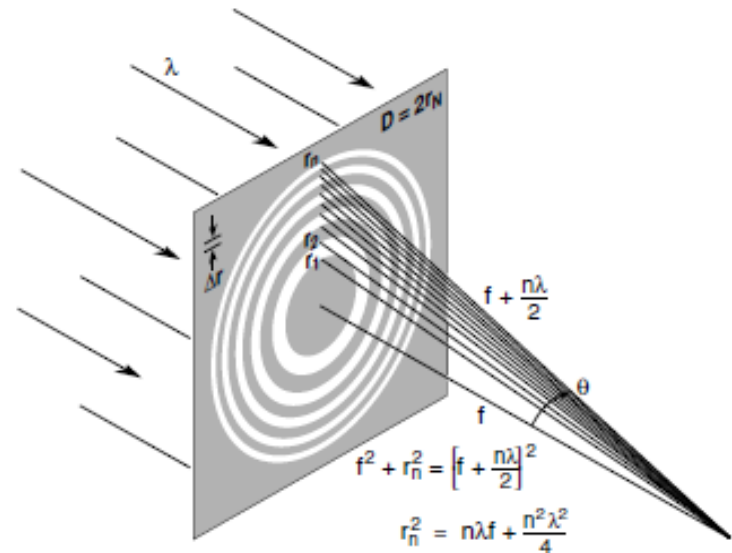
$$\text{Rayleigh res.} = \frac{0.610\lambda}{NA} = 1.22\Delta r \quad (9.47, 9.48)$$

$$\text{DOF} = \pm \frac{1}{2} \frac{\lambda}{(NA)^2} = \pm \frac{2(\Delta r)^2}{\lambda} \quad (9.50, 9.51)$$

$$\frac{\Delta\lambda}{\lambda} \leq \frac{1}{N} \quad (9.52)$$

## Pinhole Formula

$$\theta_{\text{null}} = 1.22\lambda/d \quad (9.36)$$

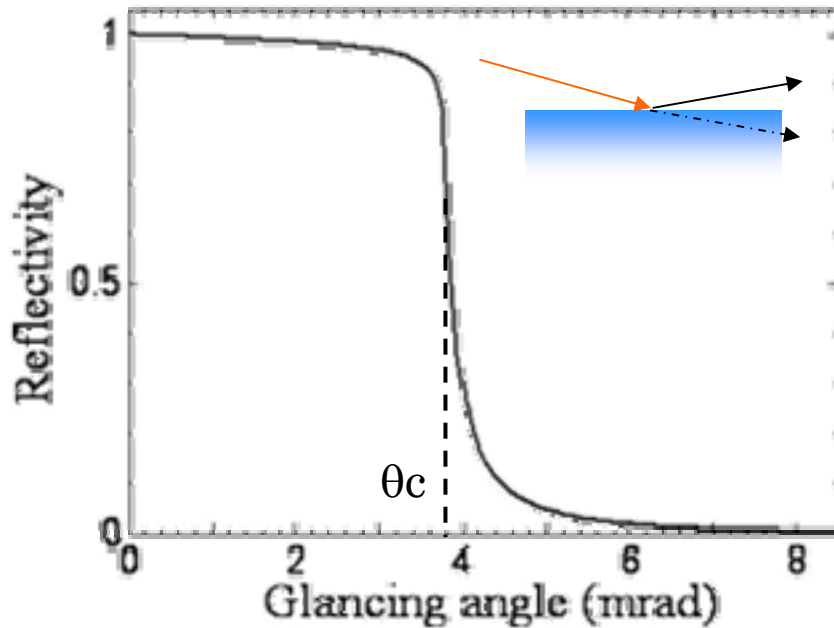


$\Delta r$ : outermost zone width  
 $N$ : total number of zones  
 $D$ : lens diameter  
 $\text{DOF}$ : Depth of Focus  
 $\Delta\lambda/\lambda$ : maximum spectral bandwidth

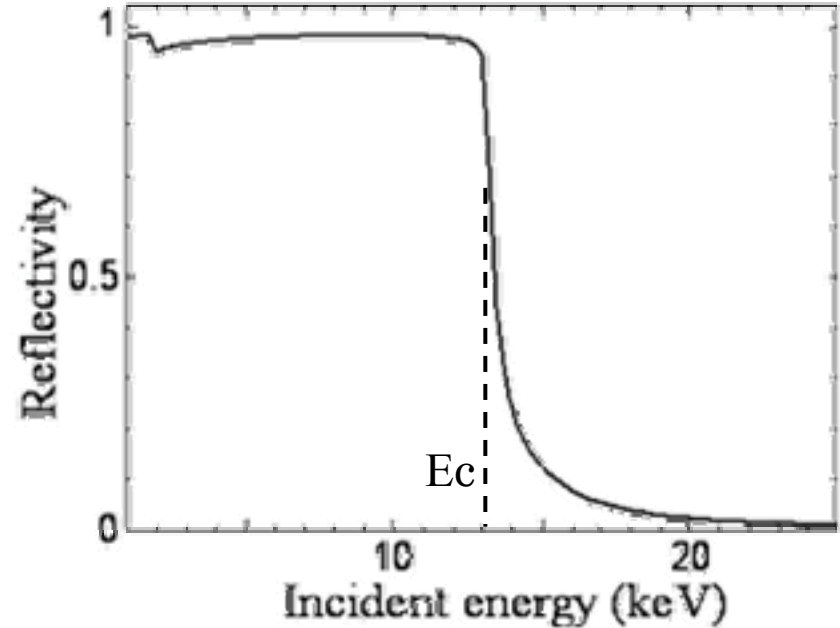


# Grazing Incidence Optics

## X-ray reflectivity for $\text{SiO}_2$ substrate



Glancing angle dependence  
for 8 keV X-rays  
( $\theta_c=3.8$  mrad).



Energy dependence for the  
glancing angle of 2.3 mrad  
( $E_c=13$  keV).

For reflectivity calculation, visit  
(CXRO) [http://henke.lbl.gov/optical\\_constants/](http://henke.lbl.gov/optical_constants/)



# Aberration of Grazing Incidence Mirror

## Aberration

- Astigmatism
- Spherical aberration
- Coma
- Chromatic aberration

EX. Spherical mirror  $1/u + 1/v = 1/f$

meridian focal length  $f_m = R \sin \theta_i / 2$

sagittal focal length  $f_s = R / 2 \sin \theta_i \Rightarrow f_m / f_s = \theta_i^2$

### Astigmatism

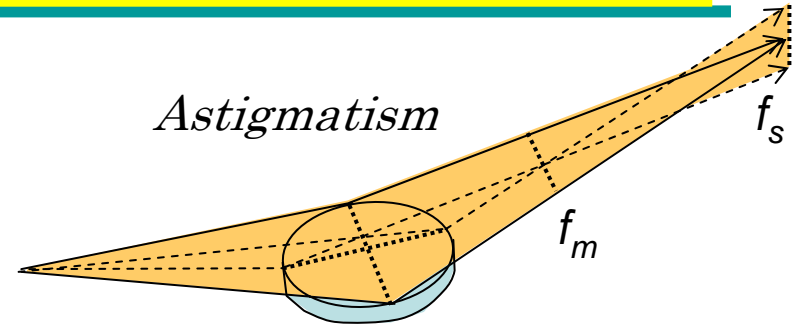
$$f_s \gg f_m$$

$$R_s = R_m \sin^2 \theta_i \quad \text{toroidal mirror (bent cylinder)}$$

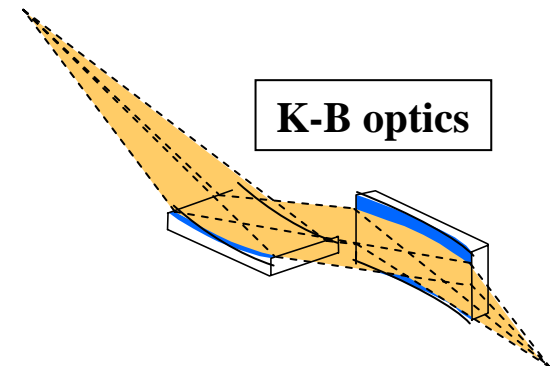
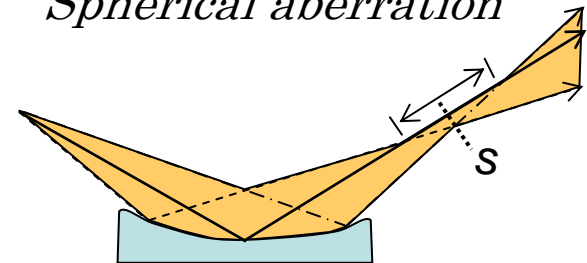
*Kirkpatrick-Baez optics*

### Spherical aberration

*elliptical / ellipsoidal mirror*

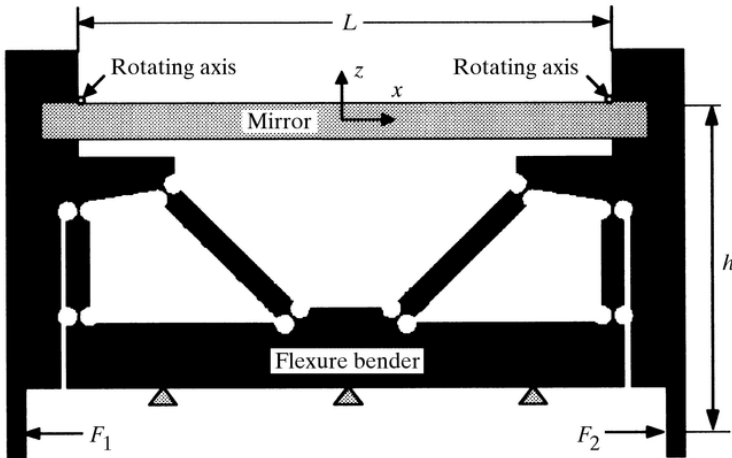


### Spherical aberration

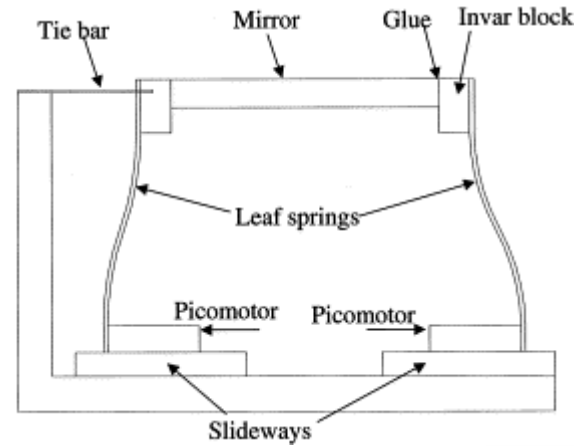




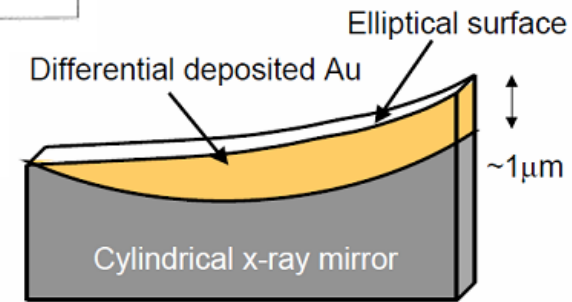
# Elliptical Mirror technology



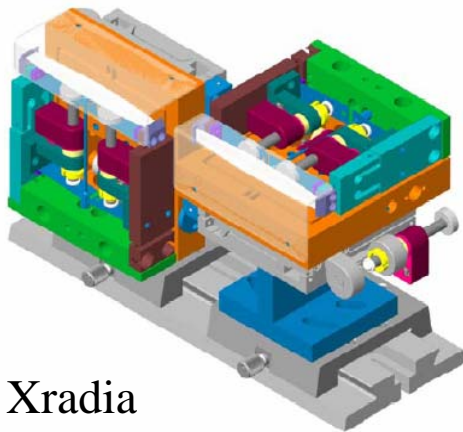
ESRF  
Flexture Hinge



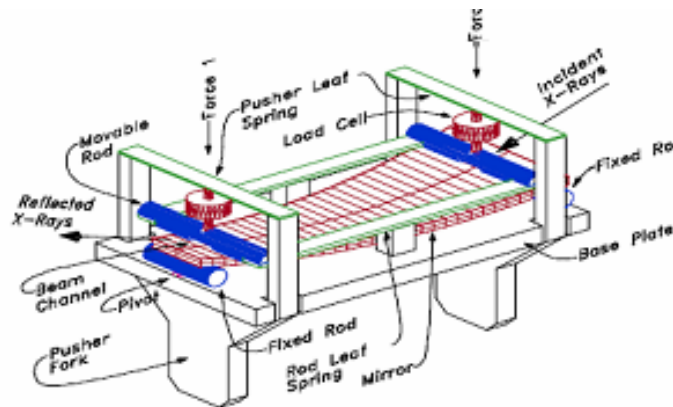
APS Leaf spring



OAK RIDGE NATIONAL LABORATORY  
U. S. DEPARTMENT OF ENERGY



Xradia  
KB-SR1



APS GeoSoilEnvironCARS



# Ultra High precision KB mirror

48 x 36nm(VxH)

By Osaka.U & SPring-8

Elastic Emission Machining  
+  
Chemical Vaporization Machining

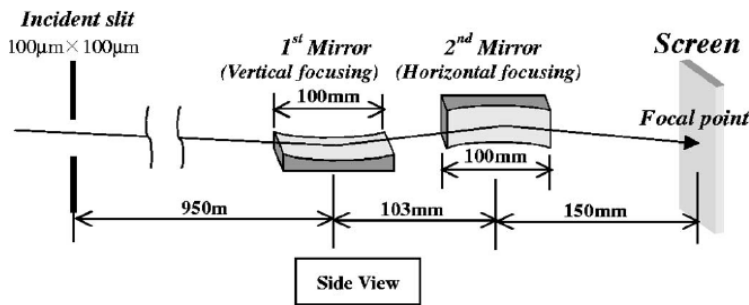


FIG. 1. Optical system using KB mirrors.

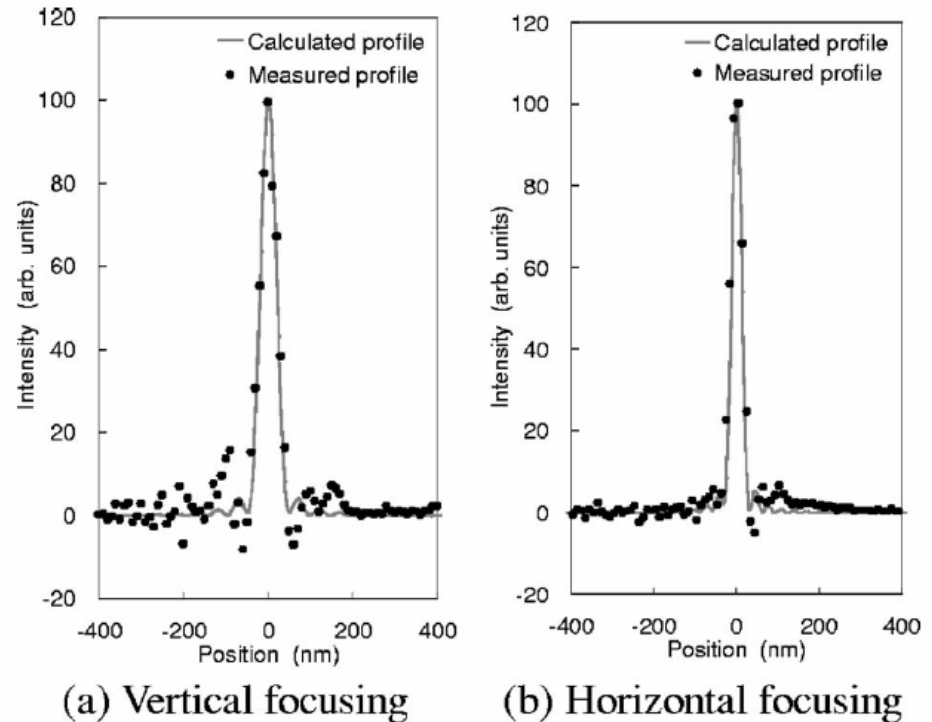


FIG. 9. Two-dimensional intensity profiles experimentally obtained, where scanning pitch is 10 nm. (a) Vertical focusing. (b) Horizontal focusing.



# Single Conical Capillary

## Conical Capillary (tapered capillary)

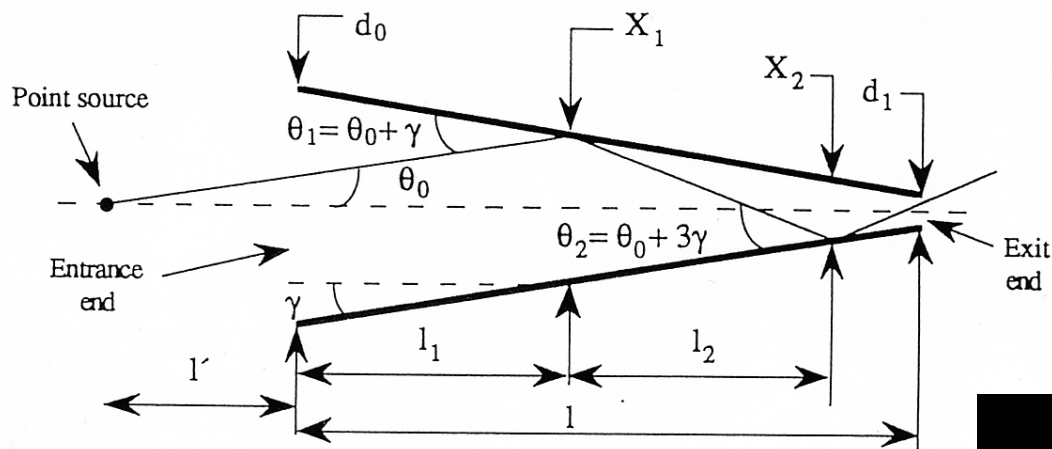
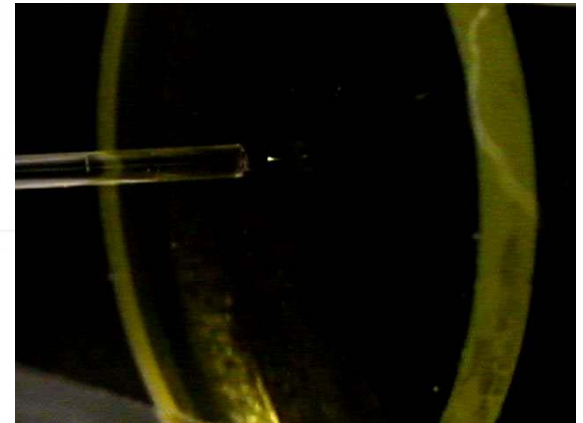


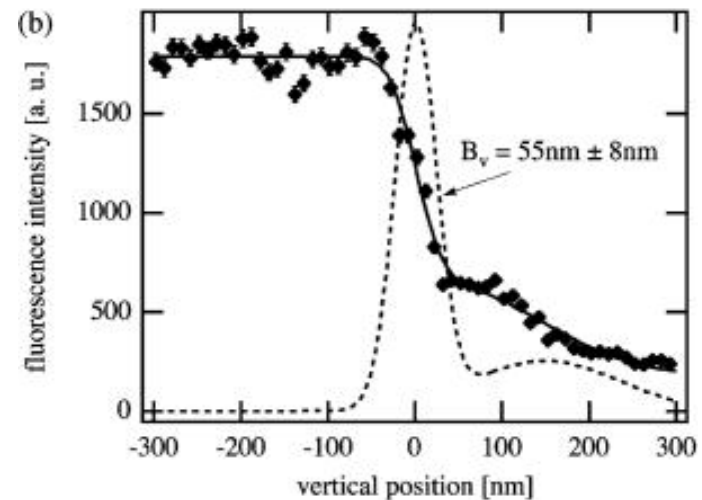
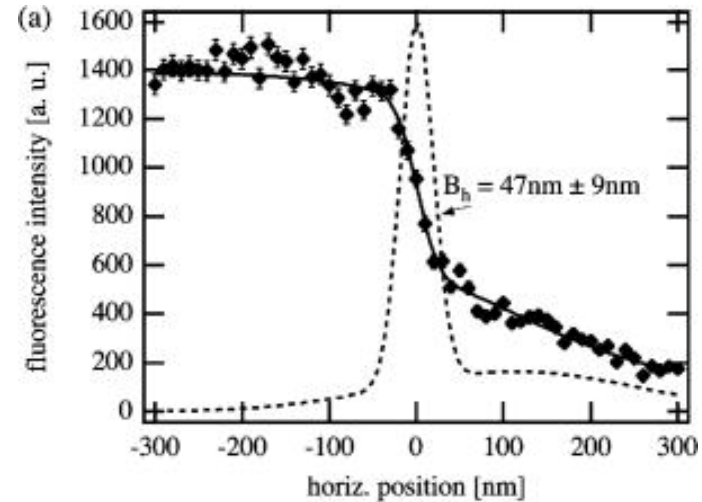
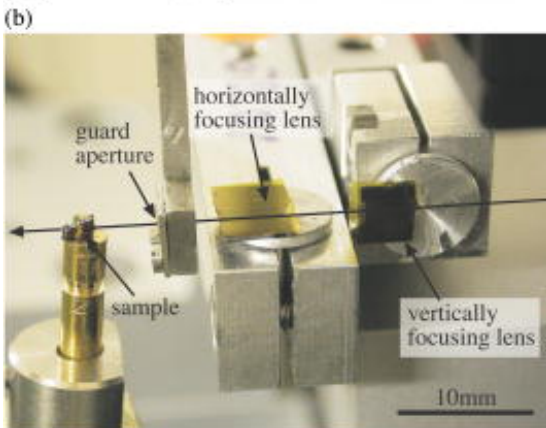
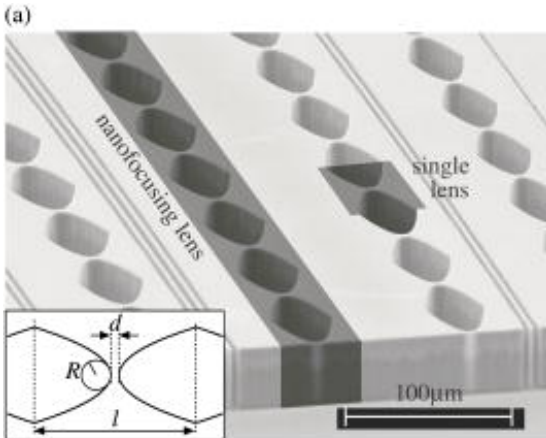
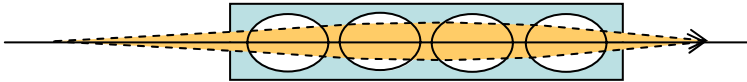
Fig III.7. Conical capillary geometry (from paper V).

After P.Engstrom



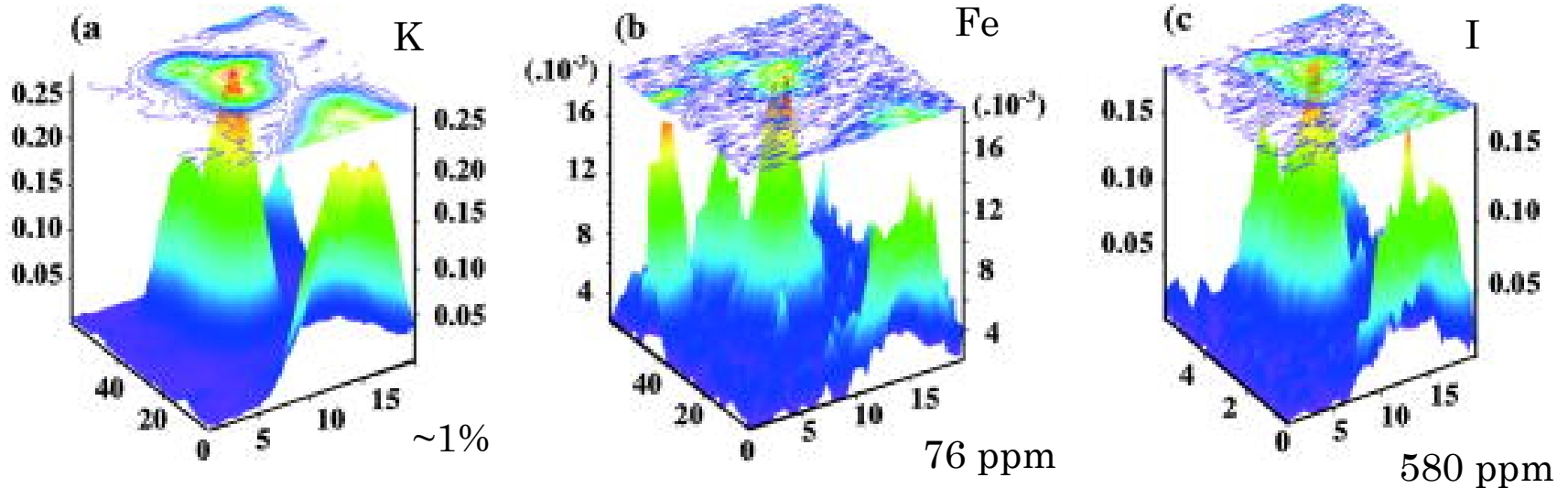


# Hard x-ray nanoprobe based on refractive x-ray lenses





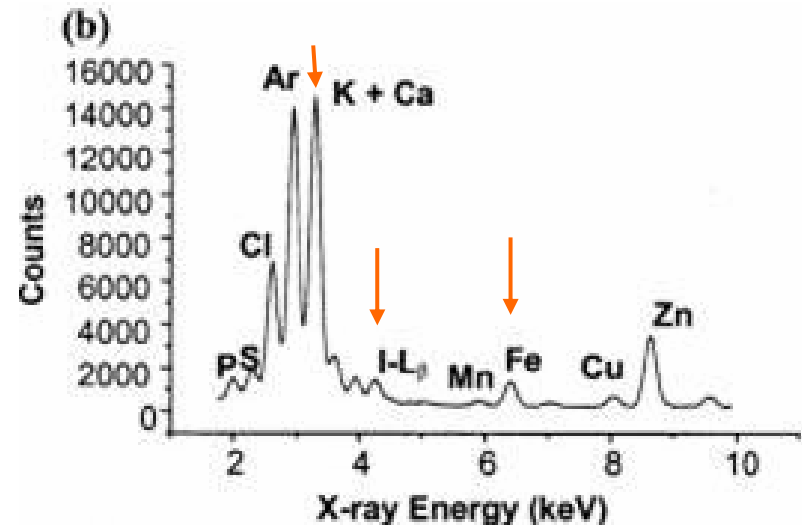
# X-ray Fluorescence imaging of single cells



a freeze-dried cancer cell treated with  $5 \mu\text{M}$  of iodo-deoxydoxorubicin(anti-cancer drug).

14 keV polychromatic pink excitation

CRL  $60 \times 60 \mu\text{m}^2$ ,  $\mu\text{g}/\text{cm}^2$



S.Bohic et al. APL 78(01)3544

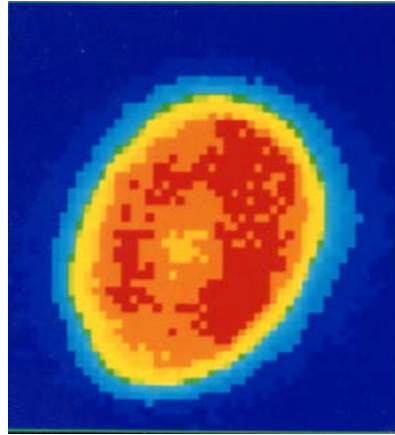


# *Human Hair Analysis*

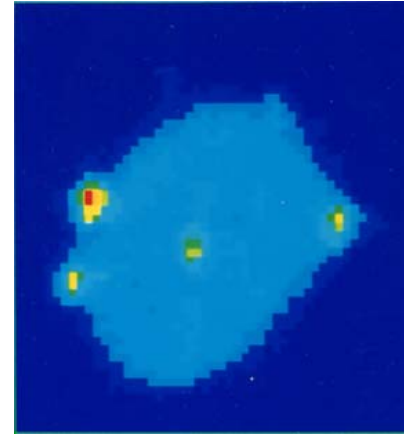
## Synchrotron X-ray Microprobe

Cross section of hair shaft,  
20mm from root end

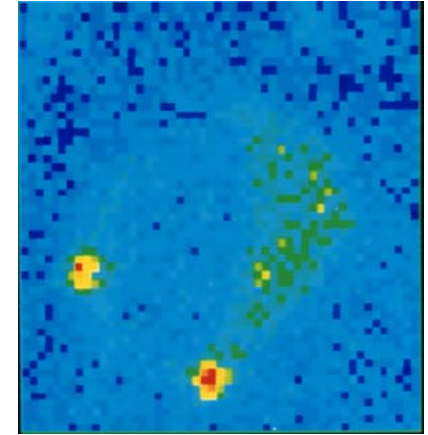
51 x 51 step  
3 $\mu$ m/step



S



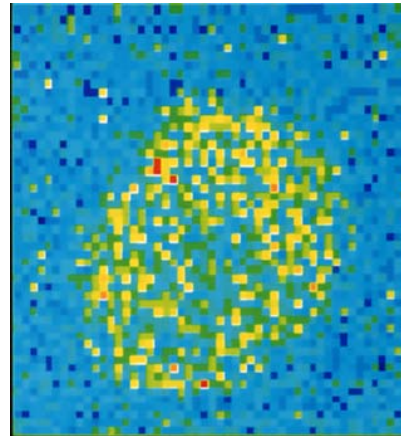
Ca



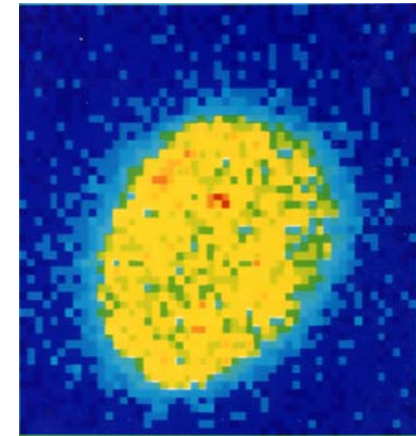
Fe



Optical micrograph



Cu



Zn



# **SRXRF Perspective**

Cheiron School 2007 by AOFSRR

A.Iida (PF)



# SRXRF perspective

- **Microbeam analysis**
  - Toward 10nm microbeam
  - Analytical SR microprobe
  - Novel Application
- **XRF imaging**
  - Micro-beam
  - Projection type
  - Micro-CT
- **Wavelength Dispersive**
  - Spectroscopy => Spectrometry  
(RIXS, MCD ....)
- **Total reflection XRF**
  - $10^8$  atoms/cm<sup>2</sup> =>  $10^6$  atoms/cm<sup>2</sup>



# SRXRF perspective

**Analytical SR Microprobe  
- Multi-detection SR microprobe -**

**$\mu$ -SRXRF**

+

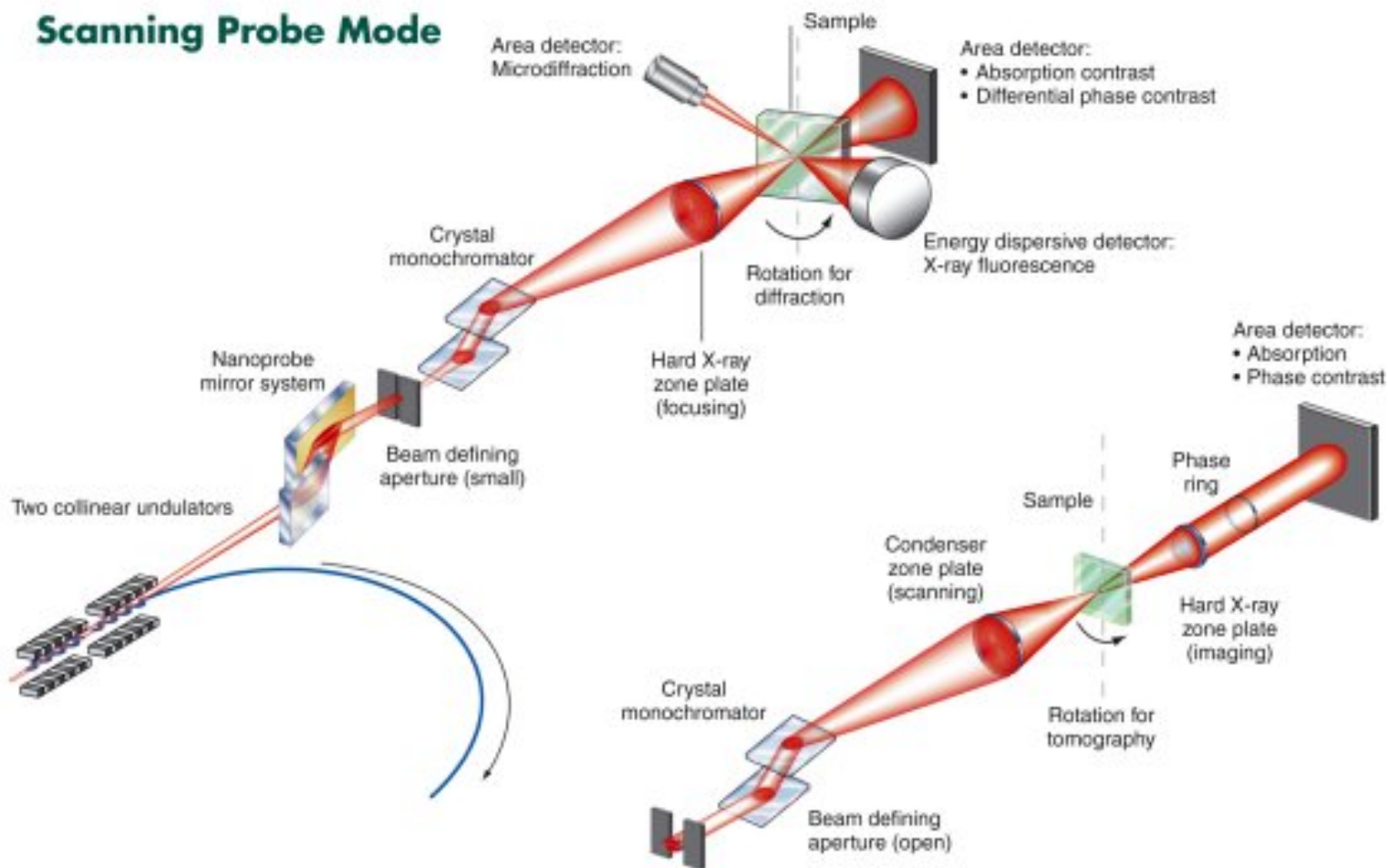
Chemical State	$\mu$ -XAFS
Local Structure	X-ray Emission
Crystal Structure	$\mu$ -XRD Poly- & Single crystal
Morphology	<b>Imaging</b> (absorption, fluorescence, phase)



# Analytical SR Microprobe

## Center for nanoscale materials @APS

### Scanning Probe Mode



### Full-Field Transmission Mode

# SR Microprobe ESRF ID22

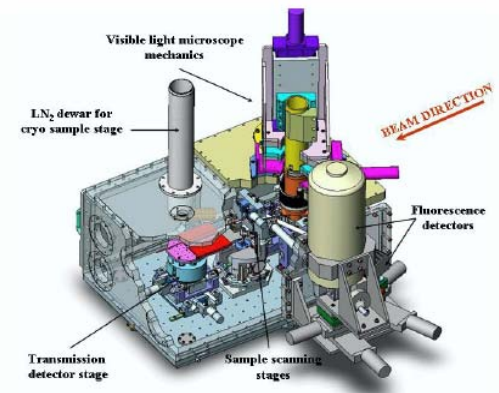
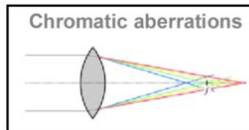
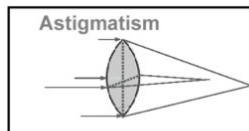
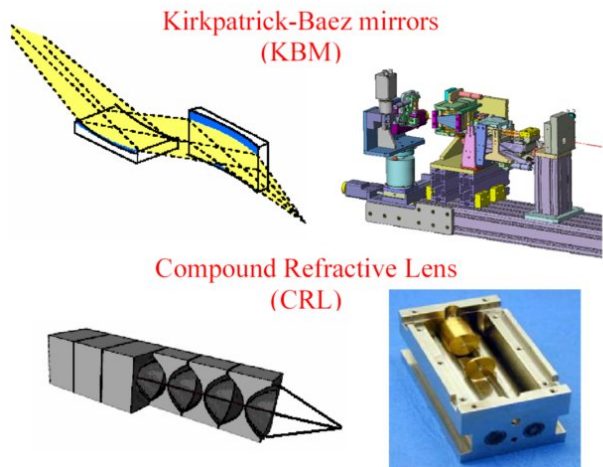
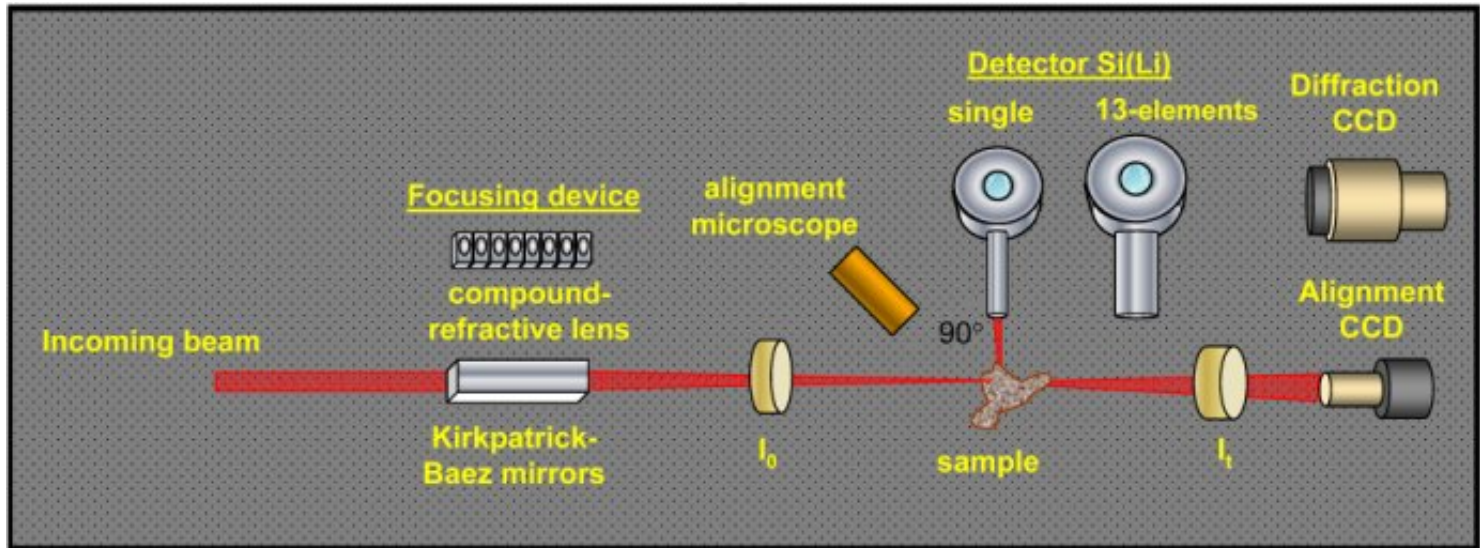


Fig. 2 Overview of the vacuum vessel and equipments of the scanning X-ray microscope of ID21.



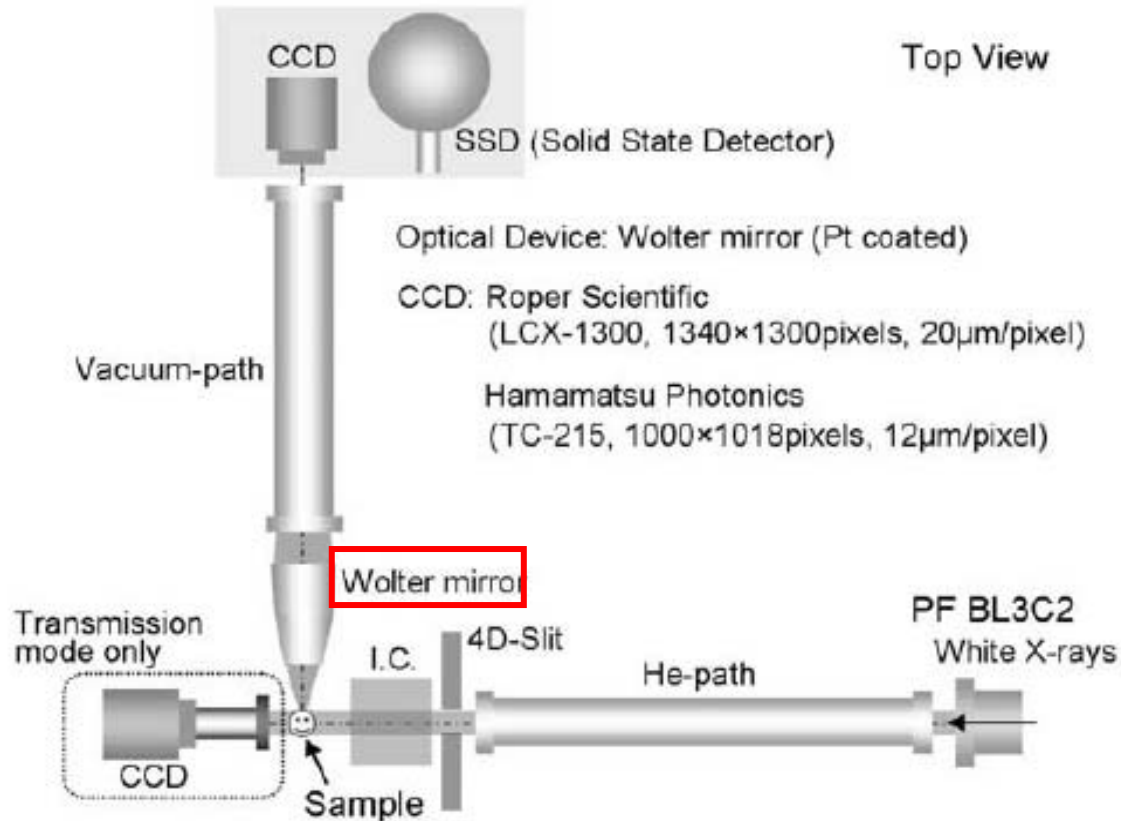
# SRXRF Imaging

---

- $\mu$ -beam Scanning
- Projection
- 3-dimensional (lateral + depth)
- Computed Tomograph



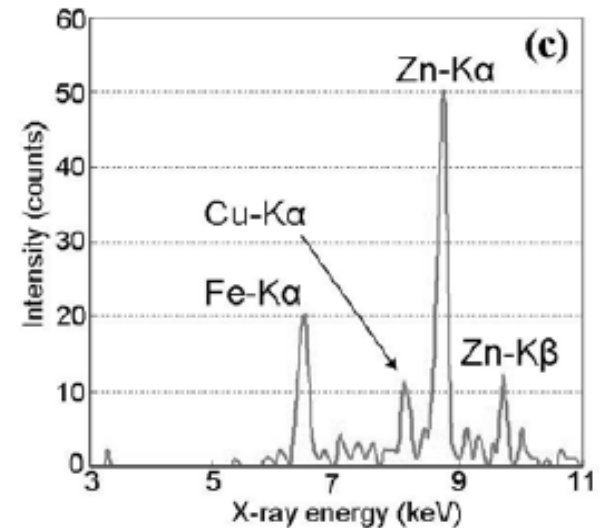
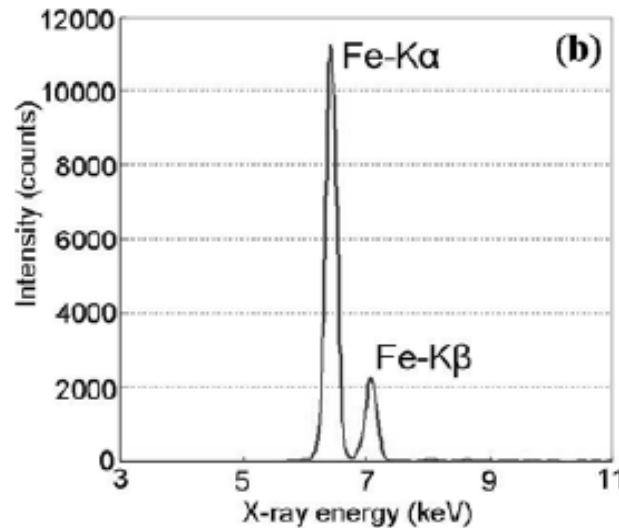
# Full-Field X-ray Fluorescence Imaging Microscope with a Wolter Mirror (1)



M.Hoshino et al. 9<sup>th</sup> SRI  
AIP Conference Proceedings 879(2007) 1283



## Full-Field X-ray Fluorescence Imaging Microscope with a Wolter Mirror (2)

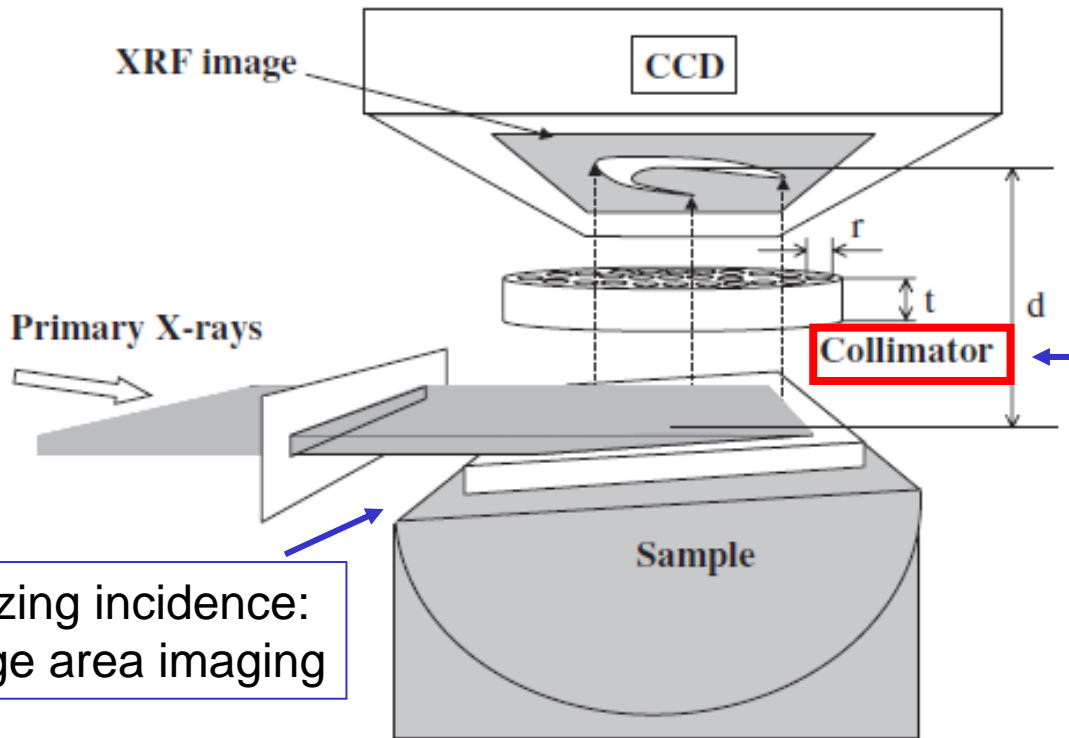


(a) X-ray fluorescence image of an **alfalfa seed**. Exp: 5 m  $\times$  12 integration.  
Bar: 0.5 mm. (CCD-2).

X-ray fluorescence energy spectra measured at (b) the luminous point and (c) the embryo. Exp: 100 s.



# Quick Projection-type XRF imaging (1)



## Advantages

- Large area ( $\sim\text{cm}^2$ )
- Quick (0.1s)
- Medium spatial resolution ( $<20\mu\text{m}$ )

Collimator:  
Selection of  
Parallel beam

Grazing incidence:  
Large area imaging

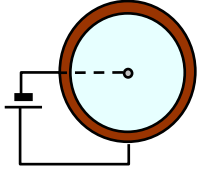
Elemental sensitivity :  
Scanning the excitation energy of  
incident X-rays

K.Sakurai, H.Eba: *Anal. Chem.*, **75**, 355 (2003).

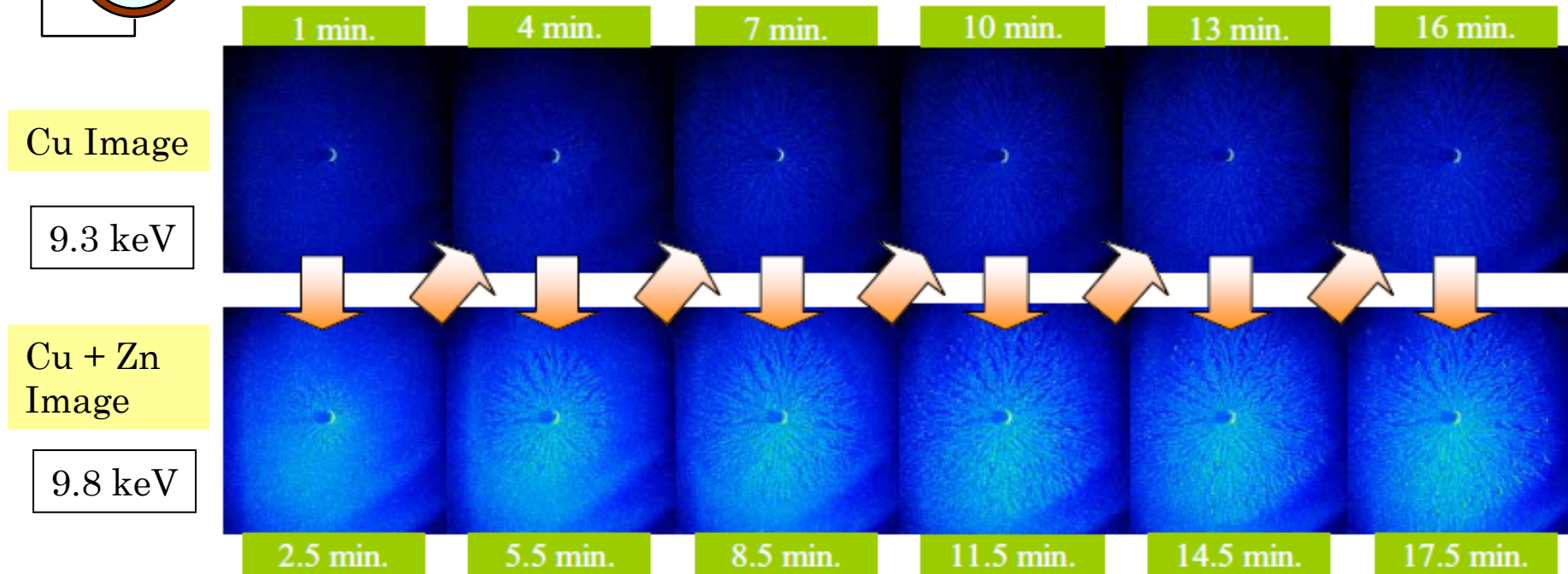


## Quick Projection-type XRF imaging (2)

Electrolysis cell



Dendrite growth during electrodeposition



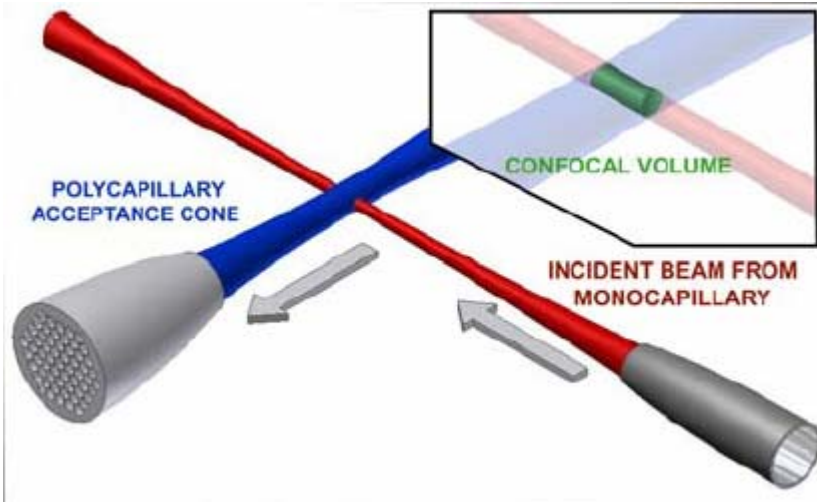
Electrodeposition from the mixed electrolyte of 0.25 mol/L  $\text{CuSO}_4$  and 0.18 mol/L  $\text{ZnSO}_4$  with 2.5 V applied voltage.

Exposure time for each image is 1 min and image size is  $12 \times 12 \text{ mm}^2$ .



# Confocal $\mu$ -XRF

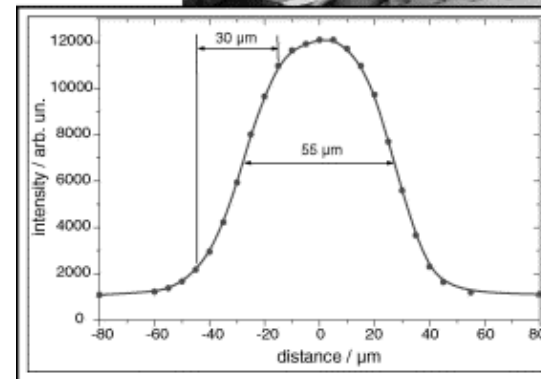
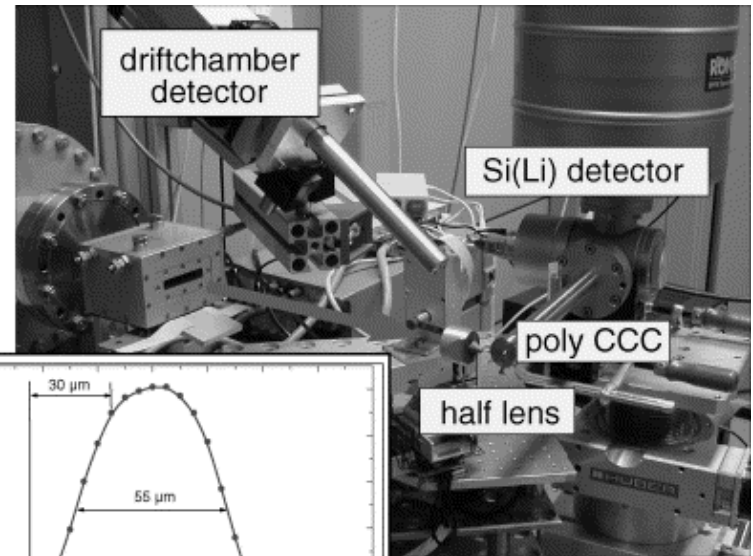
- depth profiling / 3D analysis -



A micro-volume is defined by the overlap of the foci of both X-ray optics.

Incident beam focusing can be achieved by

- Poly capillary
- Monocapillary
- CRL(refractive lens)
- ...

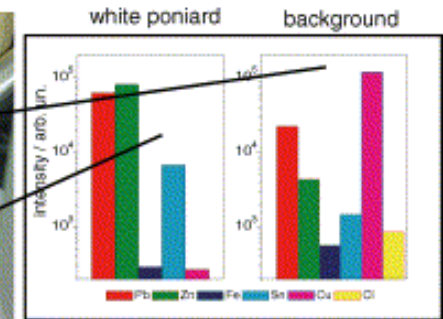
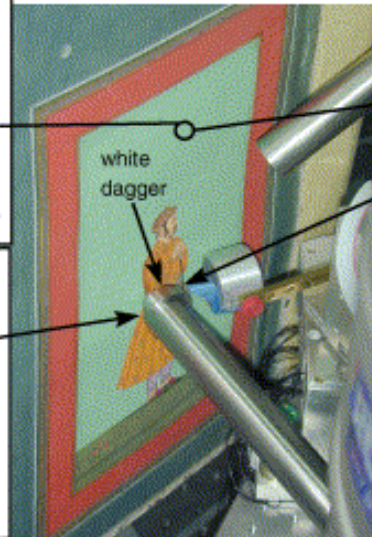
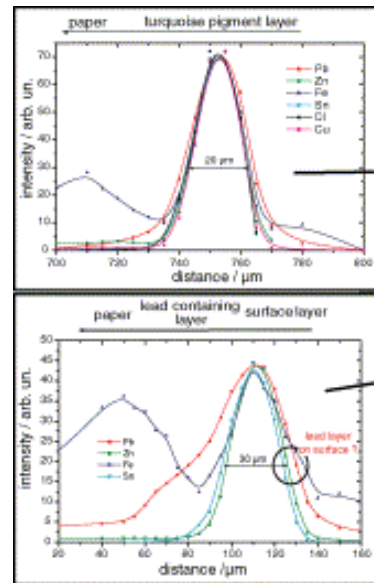
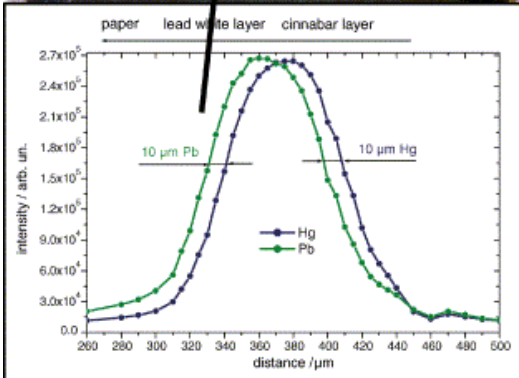
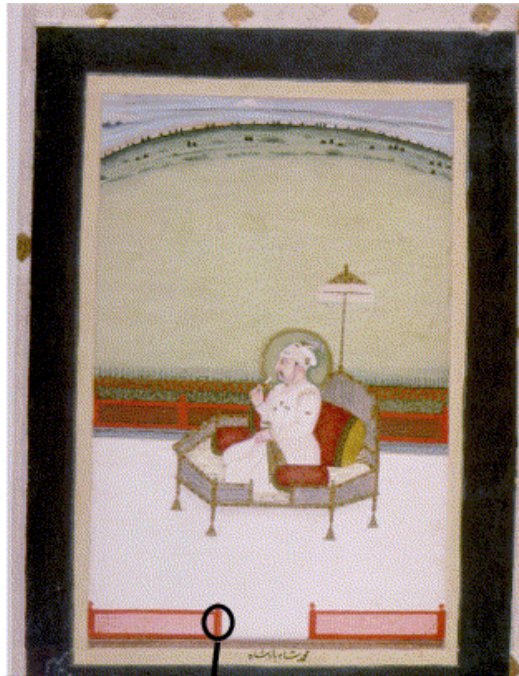


Z.Smit et al. Nucl. Instr. Methods  
B219-220 ('04)35

Hasylab, Bessy II, CHESS..



# $\mu$ -XRF depth profiling of a Mughal miniature (paint multilayer on paper)



MIK 5004 (10)  
"Abdallah Zakhmi"  
dated to the end of the 17<sup>th</sup> c.

a Mughal miniature MIK I 5004 (10) "Abdallah Zakhmi" of doubtful origin (stylistically dated to the 17th century).

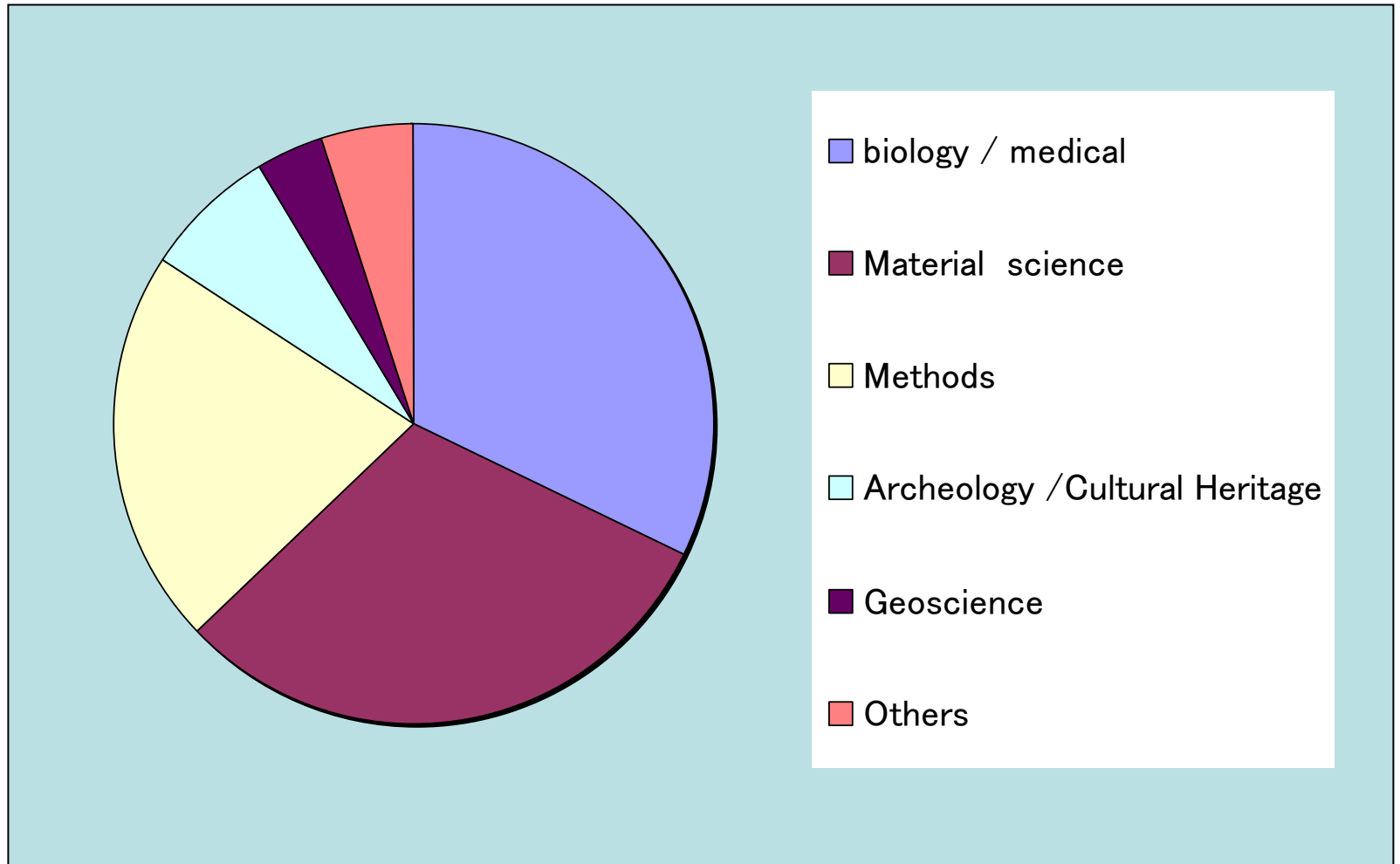
a classical Mughal miniature MIK I 5004 (3) dated from the 18th century.  
 $\text{HgS} / 2\text{PbCO}_3 \cdot \text{Pb(OH)}_2 / \text{paper}$

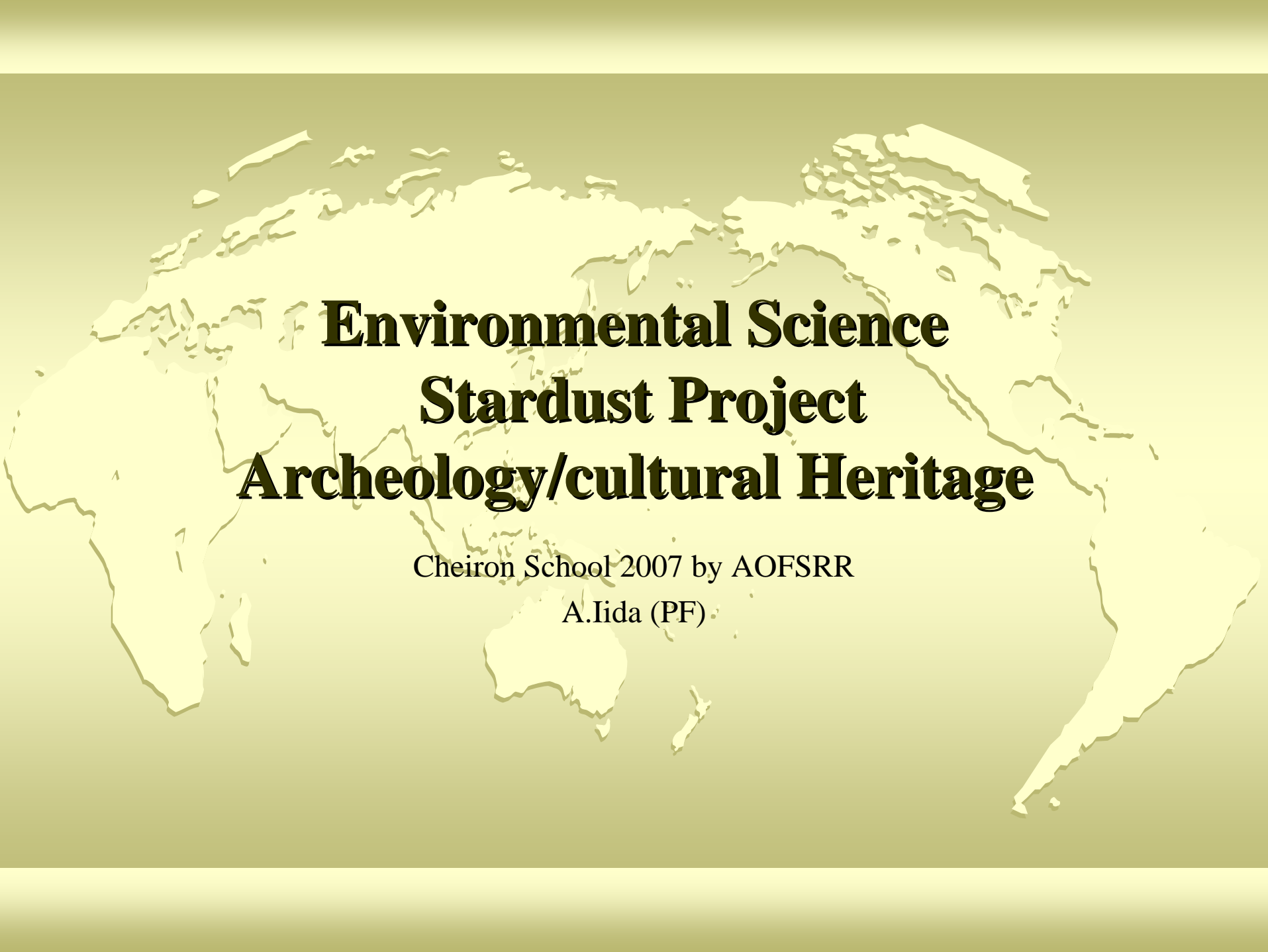
BESSY II

B.Kanngiesser et al. Nucl. Instr. Methods B211(03)259



# SRXRF related Research Fields





**Environmental Science**  
**Stardust Project**  
**Archeology/cultural Heritage**

Cheiron School 2007 by AOFSRR

A.Iida (PF)



# SRXRF Applications to Environmental Science

---

- Phytoremediation
- Aerosol Particles in Urban area
- Waste fly ash
- Uranium fuel from Chernobyl



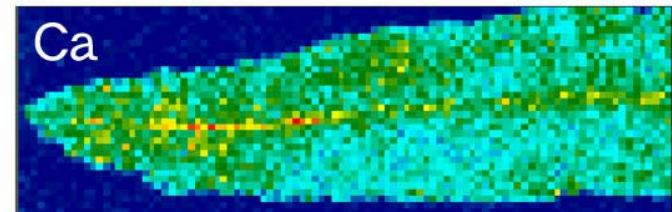
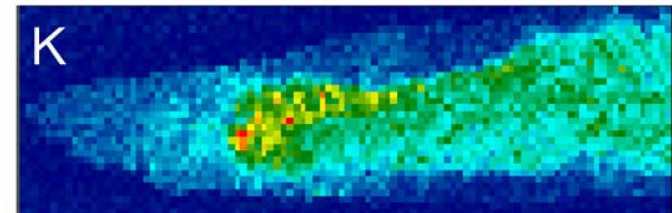
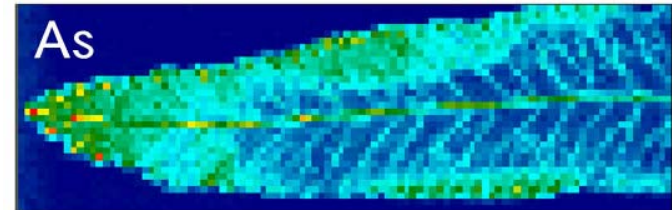
# Arsenic hyper accumulator I



The Chinese Ladder fern (*Pteris vittata*), is a highly efficient accumulator of arsenic (up to 2%).

L.Q.Ma et al. Nature 409('01) 579

Where is a hyperaccumulated element stored?  
What is the mechanism of the hyper accumulation.

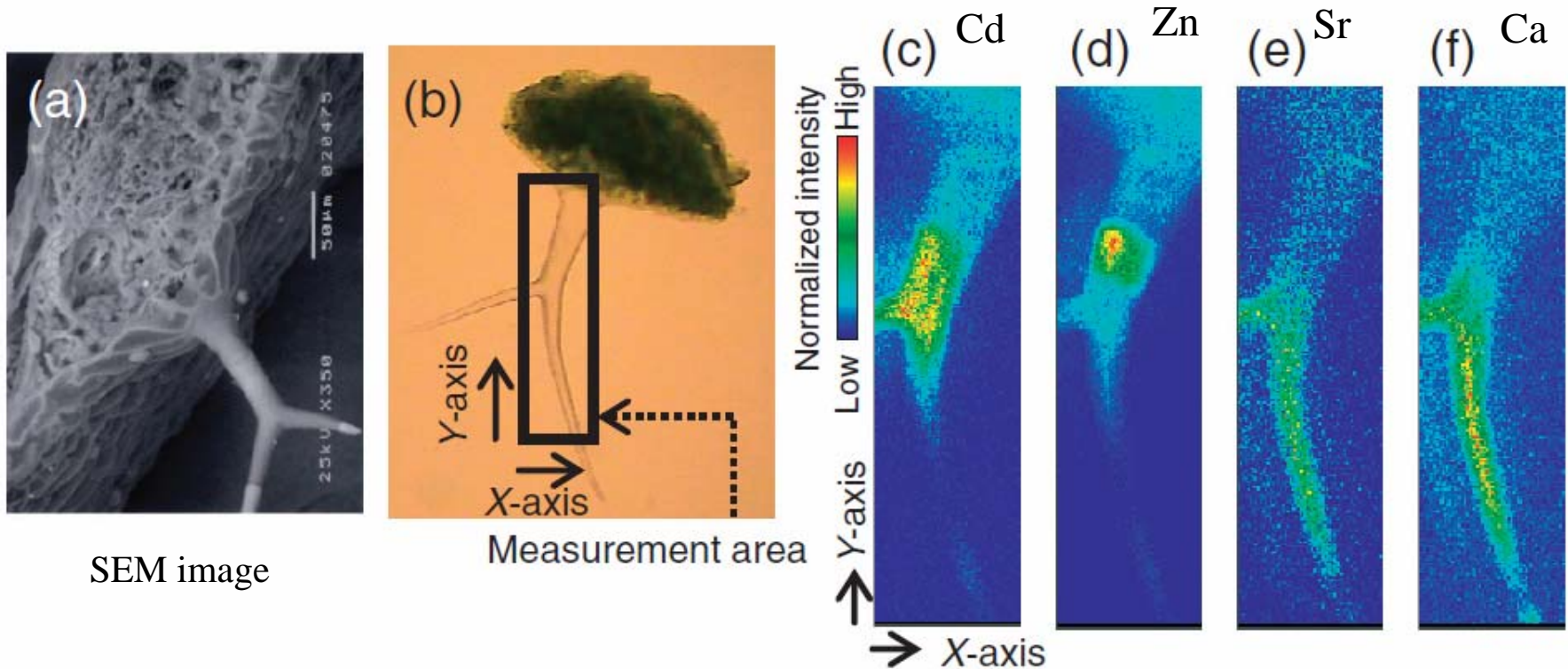


$\mu$ -XRF reveals the accumulation of As in leaf (pinna)

I.Nakai et al.  
J.Anal.Atom.Spect.(2006)



# 2-D X-ray Fluorescence Imaging of Cadmium Hyperaccumulating Plants



XRF imaging of a trichome taken from a leaf of the Cd hyper accumulating plant (*Arabidopsis halleri* ssp. *Gemmifera*).

X-ray beam size,  $3 \times 3 \mu\text{m}^2$ ; scan step,  $3 \mu\text{m}$ ; measurement time, 0.5 s/pixel; image size, 59 x 226 pixels. Cd absorption edge : 26.7 keV

A.Hokura et al. Chem. Lett. 35('06)1246 SPring-8 B137XU



# Particulate Matter (Aerosol)

Most Polluted World Cities by PM	
Particulate matter, $\mu\text{g}/\text{m}^3$ (2004)	City
169	Cairo, Egypt
150	Delhi, India
128	Kolkata, India (Calcutta)
125	Taiyuan, China
123	Chongqing, China
109	Kanpur, India
109	Lucknow, India
104	Jakarta, Indonesia
101	Shenyang, China

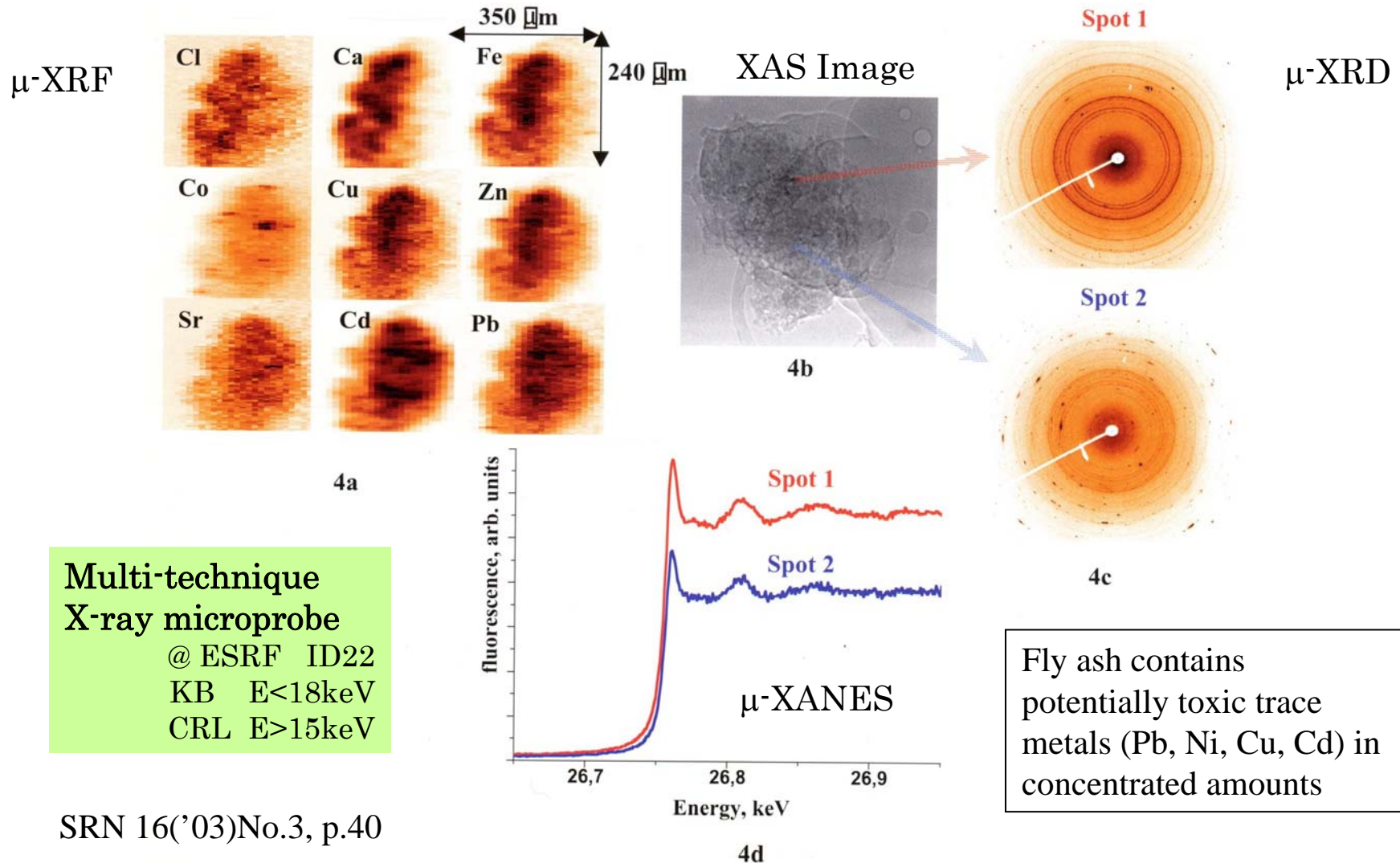
The most of them are densely populated metropolitan areas in developing countries (Wikipedia).

The primary cause the burning of fossil fuels by transportation and industrial sources.

## Effect

- Health effects
  - Asthma, Lung cancer, Cardiovascular issues, and Premature death.
  - Depending on the size of the particle
    - *PM10*: lungs, *PM2.5*, tend to penetrate into the gas-exchange regions of the lung, particles smaller than 100 nm: cell membranes
- Radiative forcing (Global warming)  
“the uncertainties relating to aerosol radiative forcings remain large.” IPCC

# Waste fly ash



Multi-technique  
X-ray microprobe  
@ ESRF ID22  
KB E<18keV  
CRL E>15keV

Fly ash contains potentially toxic trace metals (Pb, Ni, Cu, Cd) in concentrated amounts



# The origin of individual PM<sub>2.5</sub> particles in Shanghai air

PM 2.5 refers to tiny particles or droplets in the air that are 2.5  $\mu\text{m}$  or less.

Fine particles PM<sub>2.5</sub> lead to health effects and are a major cause of visibility impairment in the urban area contributing to acid rain.

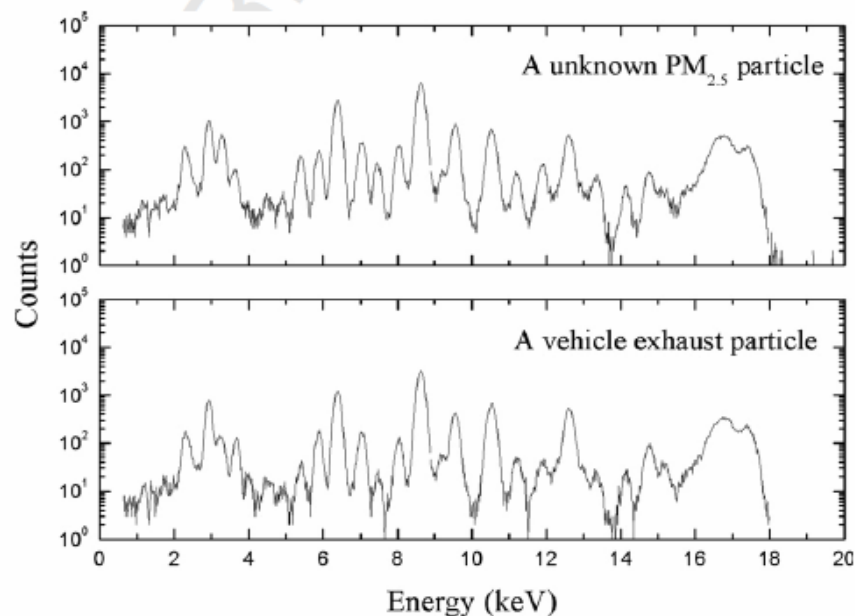


Fig. 3. A comparison of the  $\mu$ -SXRF spectrum of an unknown particle with that of a vehicle exhaust particle.

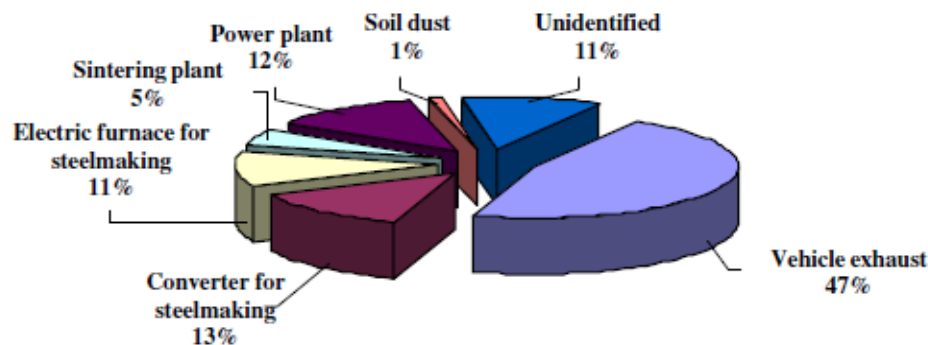
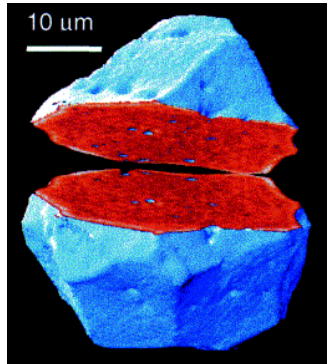


Fig. 4. Origins of the analyzed PM<sub>2.5</sub> particles collected in Shanghai air.



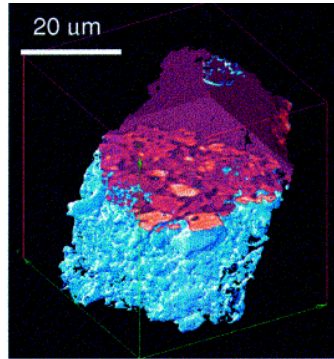
# X-ray microscopy for characterisation of fuel particles



(a)

West

μ-CT



(b)

North

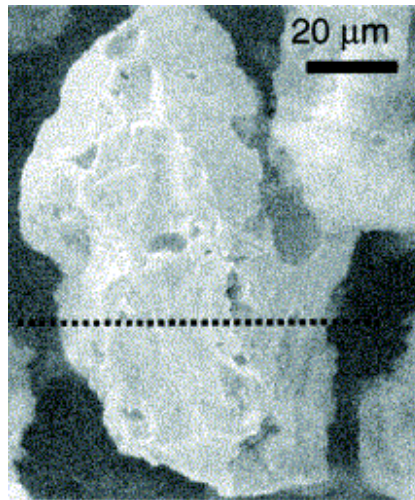
## Uranium fuel from Chernobyl (1986)

During the explosion (West)

$\text{UO}_2$ -cores with surrounding layer of reduced U with low weathering rates.

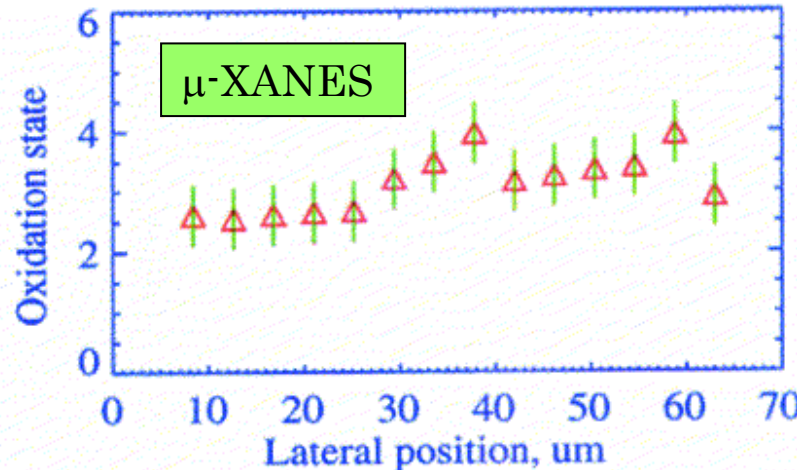
During the subsequent fire (North)

$\text{UO}_2$ -core with surrounding layers of oxidised  $\text{U}_2\text{O}_5/\text{U}_3\text{O}_8$  with high weathering rates



(a)

SEM



West:reduced U

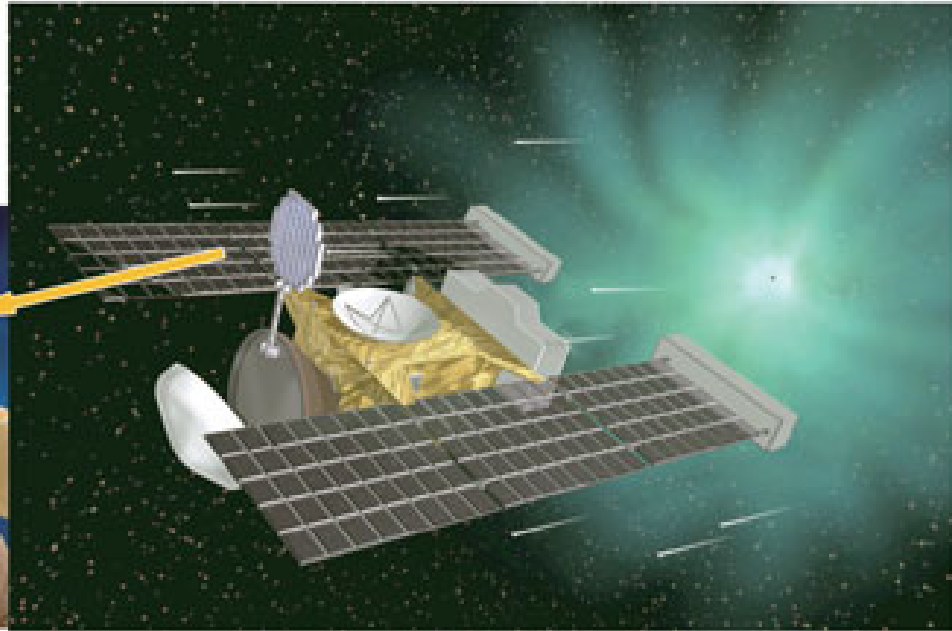
μ-CT  
μ-XRD  
μ-XANES



# *Stardust Project*

NASA's Comet Sample Return Mission

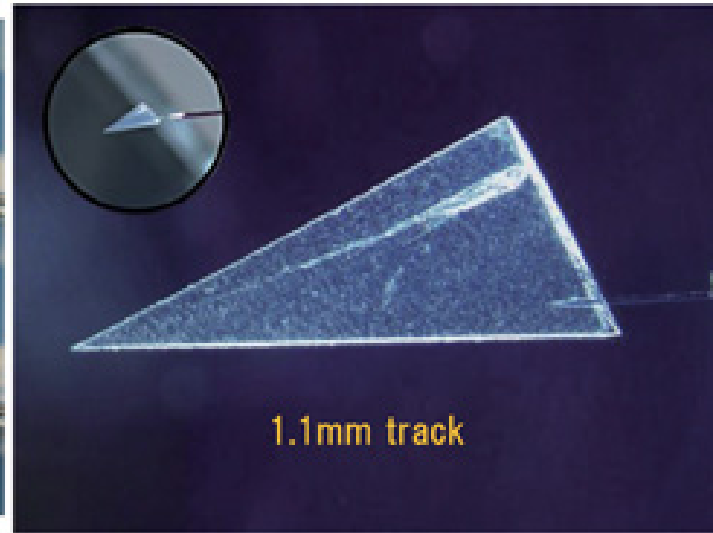
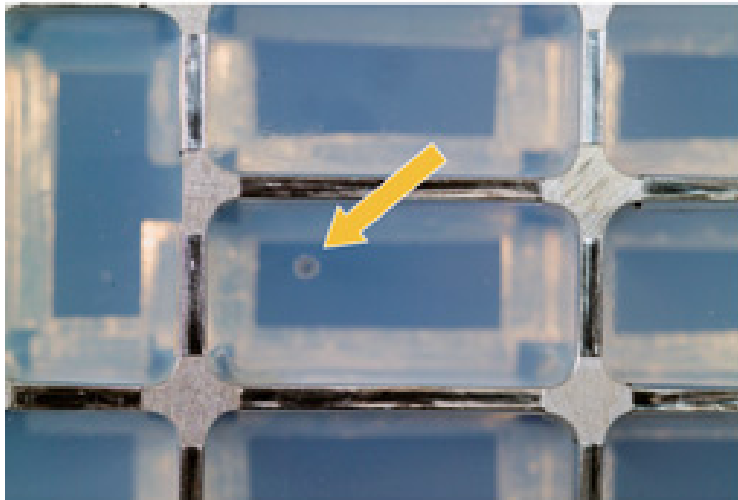
The capture of  
comet dust within  
aerogel



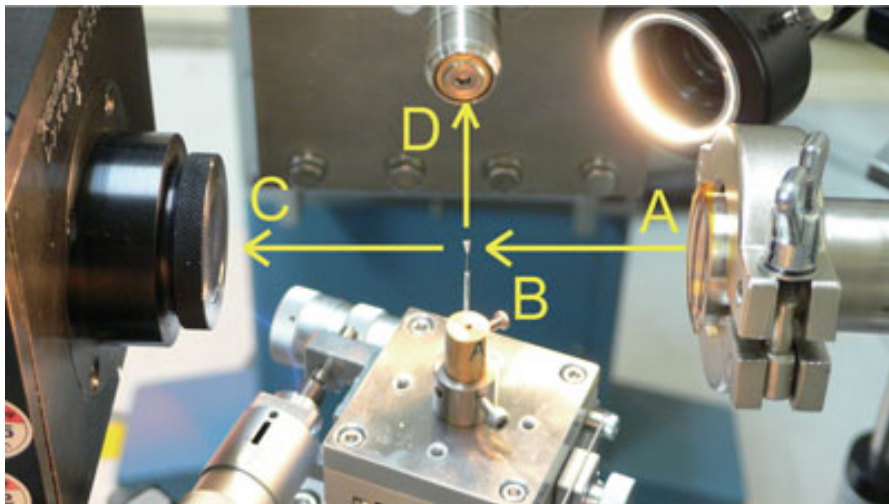
The Stardust mission was launched into space in early February 1999. Its destination - Comet Wild 2; its mission, to capture cometary materials before returning to earth in 2006.



# Stardust Project (NASA)



Stardust track  
in Aerogel



X-ray CT and XRF

@SPring-8

[http://www.spring8.or.jp/ja/current\\_result/SPring8News/no\\_33](http://www.spring8.or.jp/ja/current_result/SPring8News/no_33)



# As many as 80 researchers involved!

REPORT

## Elemental Compositions of Comet 81P/Wild 2 Samples Collected by Stardust

George J. Flynn,<sup>1\*</sup> Pierre Bleuett,<sup>2</sup> Janet Borg,<sup>3</sup> John P. Bradley,<sup>4</sup> Frank E. Brenker,<sup>5</sup> Sean Brennan,<sup>6</sup> John Bridges,<sup>7</sup> Don E. Brownlee,<sup>8</sup> Emma S. Bullock,<sup>9</sup> Manfred Burghammer,<sup>2</sup> Benton C. Clark,<sup>10</sup> Zu Rong Dai,<sup>4</sup> Charles P. Daghljan,<sup>11</sup> Zahia Djouadi,<sup>3</sup> Sirine Fakra,<sup>12</sup> Tristan Ferroir,<sup>13</sup> Christine Floss,<sup>14</sup> Ian A. Franchi,<sup>7</sup> Zack Gainsforth,<sup>15</sup> Jean-Paul Gallien,<sup>16</sup> Philippe Gillet,<sup>13</sup> Patrick G. Grant,<sup>4</sup> Giles A. Graham,<sup>4</sup> Simon F. Green,<sup>7</sup> Faustine Grossemy,<sup>3</sup> Philipp R. Heck,<sup>17</sup> Gregory F. Herzog,<sup>18</sup> Peter Hoppe,<sup>17</sup> Friedrich Hörz,<sup>19</sup> Joachim Huth,<sup>17</sup> Konstantin Ignatyev,<sup>6</sup> Hope A. Ishii,<sup>4</sup> Koen Janssens,<sup>20</sup> David Joswiak,<sup>8</sup> Anton T. Kearsley,<sup>21</sup> Hicham Khodja,<sup>16</sup> Antonio Lanzirotti,<sup>22</sup> Jan Leitner,<sup>23</sup> Laurence Lemelle,<sup>13</sup> Hugues Leroux,<sup>24</sup> Katharina Luening,<sup>6</sup> Glenn J. MacPherson,<sup>9</sup> Kuljeet K. Marhas,<sup>14</sup> Matthew A. Marcus,<sup>12</sup> Graciela Matrajt,<sup>8</sup> Tomoki Nakamura,<sup>25</sup> Keiko Nakamura-Messenger,<sup>26</sup> Tsukasa Nakano,<sup>27</sup> Matthew Newville,<sup>22</sup> Dimitri A. Papanastassiou,<sup>28</sup> Piero Pianetta,<sup>6</sup> William Rao,<sup>29</sup> Christian Riekel,<sup>2</sup> Frans J. M. Rietmeijer,<sup>30</sup> Detlef Rost,<sup>9</sup> Craig S. Schwandt,<sup>26</sup> Thomas H. See,<sup>26</sup> Julie Sheffield-Parker,<sup>31</sup> Alexandre Simionovici,<sup>13</sup> Ilona Sitnitsky,<sup>1</sup> Christopher J. Sneed,<sup>15</sup> Frank J. Stadermann,<sup>14</sup> Thomas Stephan,<sup>23</sup> Rhonda M. Stroud,<sup>32</sup> Jean Susini,<sup>2</sup> Yoshio Suzuki,<sup>33</sup> Stephen R. Sutton,<sup>22</sup> Susan Taylor,<sup>34</sup> Nick Teslich,<sup>4</sup> D. Troadec,<sup>24</sup> Peter Tsou,<sup>28</sup> Akira Tsuchiyama,<sup>35</sup> Kentaro Uesugi,<sup>33</sup> Bart Vekemans,<sup>20</sup> Edward P. Vicenzi,<sup>9</sup> Laszlo Vincze,<sup>36</sup> Andrew J. Westphal,<sup>15</sup> Penelope Wozniakiewicz,<sup>21</sup> Ernst Zinner,<sup>14</sup> Michael E. Zolensky<sup>19</sup>

We measured the elemental compositions of material from 23 particles in aerogel and from residue in seven craters in aluminum foil that was collected during passage of the Stardust spacecraft through the coma of comet 81P/Wild 2. These particles are chemically heterogeneous at the largest size scale analyzed (~180 ng). The mean elemental composition of this Wild 2 material is consistent with the CI meteorite composition, which is thought to represent the bulk composition of the solar system, for the elements Mg, Si, Mn, Fe, and Ni to 35%, and for Ca and Ti to 60%. The elements Cu, Zn, and Ga appear enriched in this Wild 2 material, which suggests that the CI meteorites may not represent the solar system composition for these moderately volatile minor elements.

**N**ASA's Stardust spacecraft collected dust particles from comet 81P/Wild 2, at an encounter speed of ~6.1 km/s, in silica aerogel capture cells and in impact craters (1). Analytical results from the aerogel and foils were combined to provide a more comprehensive elemental analysis of the Wild 2 particles.

The impacts in aerogel produced elongated cavities called tracks. Wedges of aerogel, called keystones (2), containing an entire track were extracted. The volume containing each track was analyzed by means of synchrotron-based x-ray microprobes (SXRMs), providing abundances for elements having an atomic number  $Z \geq 16$  (S). One

track was subsequently split open, exposing the wall for time-of-flight-secondary ion mass spectrometry (TOF-SIMS) analysis, detecting lower-Z elements, particularly Mg and Al. Because Si and O are the major elements in silica aerogel, neither element could be determined in the comet material in tracks. The residues in craters were analyzed by scanning electron microscopy using energy-dispersive x-ray (SEM-EDX) analyses and TOF-SIMS, providing other element abundances, including Mg and Si.

The SXRMs produce intense, focused beams of x-rays that completely penetrate a keystone, exciting fluorescence (3). Elemental analysis was performed on keystones containing 23 tracks, which were selected to sample the diversity on the collector, by seven research groups with the use of six different SXRMs (4). These tracks range in length from ~250  $\mu\text{m}$  to almost 10,000  $\mu\text{m}$  and vary in shape from conical to bulbous. The Fe content of the tracks varies from ~180 fg to 6.4 ng (table S3), comparable to the Fe in chondritic particles ranging from ~1 to ~30  $\mu\text{m}$  in size. All 23 tracks were approximately normal to the aerogel surface, which was the arrival direction for particles collected from Wild 2 (1), whereas interplanetary particles, also collected, arrived over a wide range of orientations. Comets are thought to preserve dust from the early solar system, so we compared the Wild 2 dust to the elemental composition of the CI meteorites (CI) (5) because CI is thought to represent the nonvolatile composition of the solar system (6).

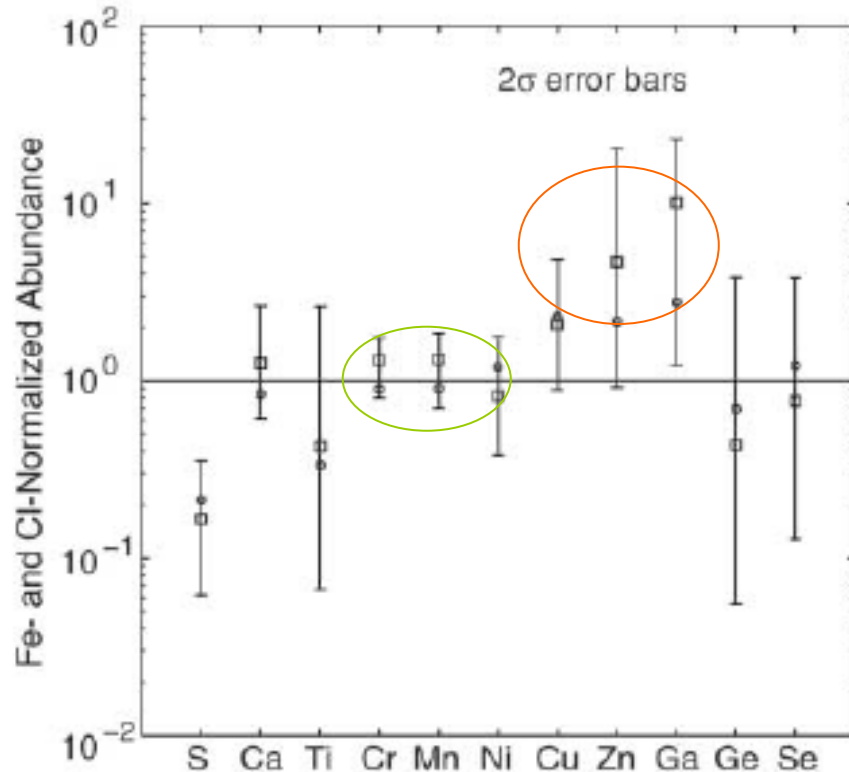
A map of the K-alpha fluorescence intensity for Fe from a conical track, track 19, shows that the incident particle deposited Fe along much of the entry path (Fig. 1), with only 3% of the total Fe contained in the terminal particle. The fraction of the total Fe detected in the terminal particle varies from track to track, ranging from almost 60% in one terminal particle to zero in two tracks having no detectable terminal particle. In most of the 23 tracks, most of the incident Fe mass is unevenly distributed along the track, indicating that the

ALS,APS,  
NSLS, SSRL  
+  
Spring-8, ESRF

Downloaded from www.sciencemag.org on August 1



# CI- and Fe-normalized mean composition



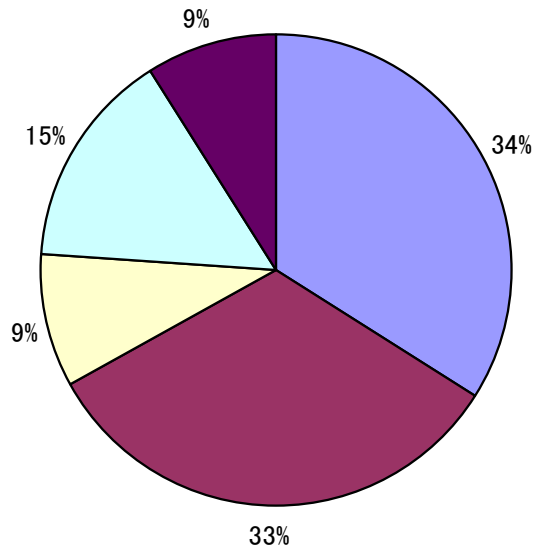
## Summary

The mean elemental composition of this Wild 2 material is consistent with the CI meteorite composition, which is thought to represent the bulk composition of the solar system, for the elements Mg, Si, Mn, Fe, and Ni to 35%, and for Ca and Ti to 60%. The elements Cu, Zn, and Ga appear enriched in this Wild 2 material, which suggests that the CI meteorites may not represent the solar system composition for these moderately volatile minor elements.



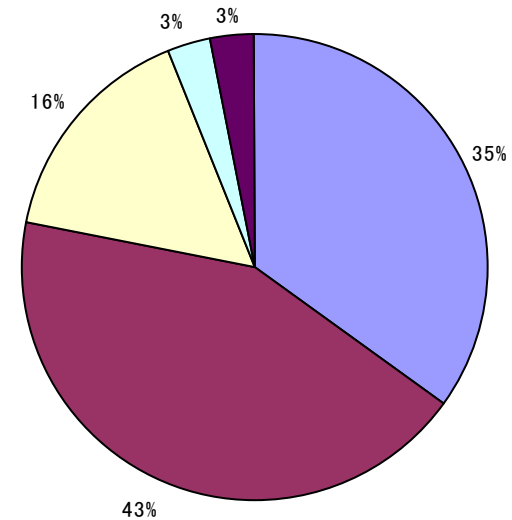
# SR in Archeology and Cultural Heritage

## Materials studied



- pigment, painting, parchment, textile
- ceramic, glaze, glass
- metal, corrosion
- bone, teeth, hair

## SR techniques used



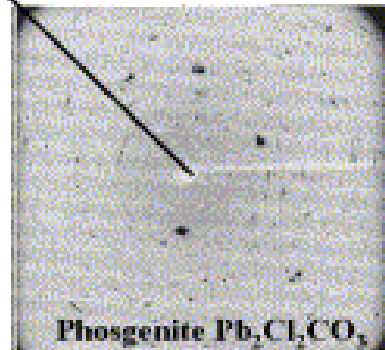
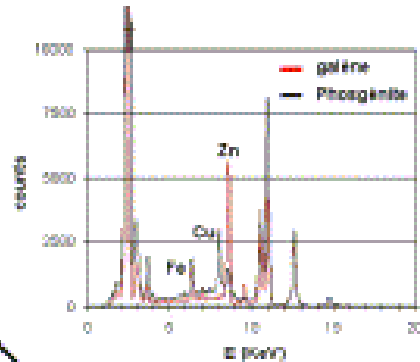
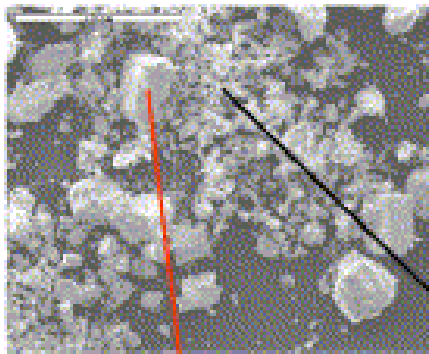
- XRF
- XRD
- XAFS
- IR
- SAXS



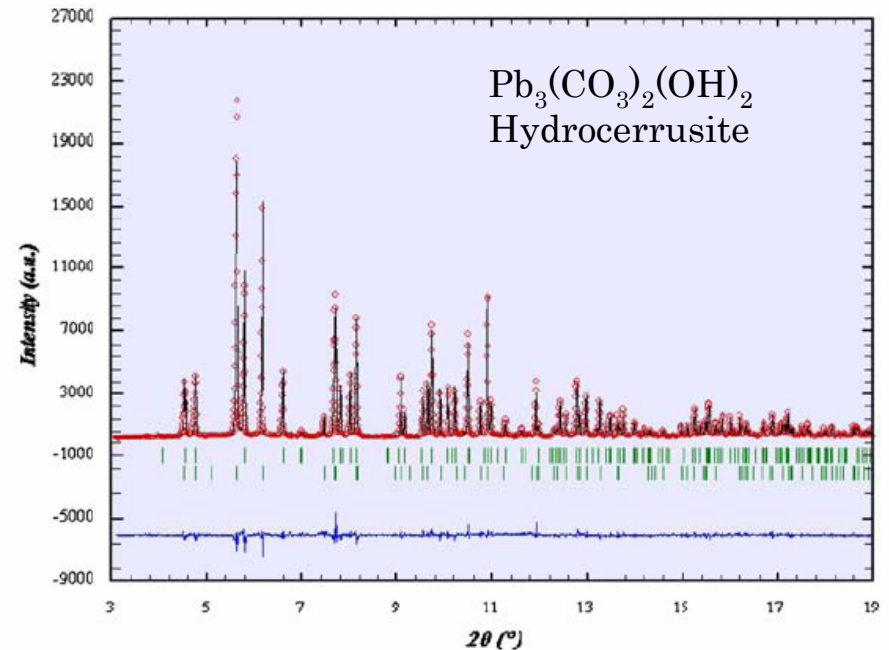
# Egyptian Chemicals (cosmetics)

Cosmetic powders in 52 make-up containers  
@ the Louvre Museum  
 $\mu$ -XRF +  $\mu$ -XRD @ESRF ID22

Origin of the materials  
(crystal structure + impurity pattern)

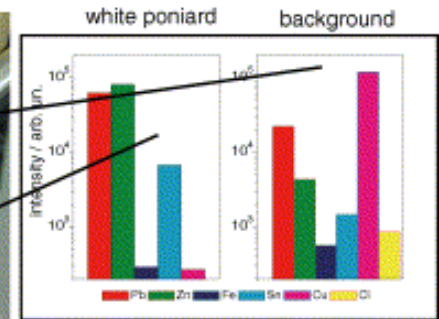
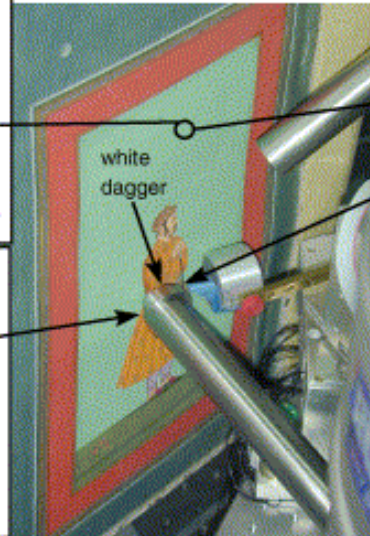
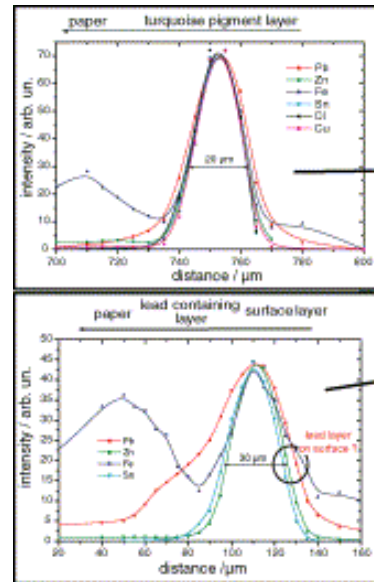
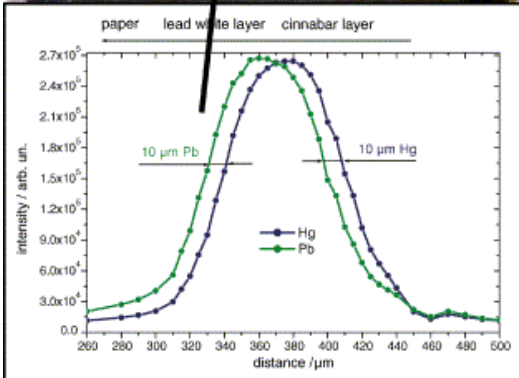
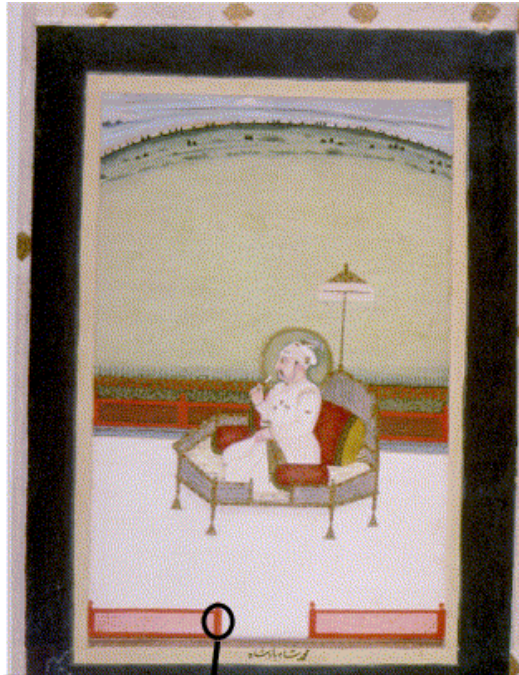


Phase structure determination  
using the Rietveld refinement





# $\mu$ -XRF depth profiling of a Mughal miniature (paint multilayer on paper)



MIK 5004 (10)  
"Abdallah Zakhmi"  
dated to the end of the 17<sup>th</sup> c.

a Mughal miniature MIK I 5004 (10) "Abdallah Zakhmi" of doubtful origin (stylistically dated to the 17th century).

a classical Mughal miniature  
MIK I 5004 (3) dated from the  
18th century.  
 $\text{HgS} / 2\text{PbCO}_3 \cdot \text{Pb}(\text{OH})_2 / \text{paper}$

BESSY II

B.Kanngiesser et al. Nucl. Instr. Methods B211(03)259



# SRXRF perspective

- **Microbeam analysis**
  - Toward 10nm microbeam
  - Analytical SR microprobe
  - Novel Application
- **XRF imaging**
  - Micro-beam
  - Projection type
  - Micro-CT
- **Wavelength Dispersive**
  - Spectroscopy => Spectrometry  
(RIXS, MCD ....)
- **Total reflection XRF**
  - $10^8$  atoms/cm<sup>2</sup> =>  $10^6$  atoms/cm<sup>2</sup>

If you have any questions about SRXRF please contact:

Atsuo IIDA  
Photon Factory  
Atsuo.iida@kek.jp